altered either by chronic insulin treatment, treatment with rapamycin, or expression of ΔIP-SHIP2 and IRS-1 (Fig. 4b).

Effect of ΔIP-SHIP2 and IRS-1 expression, and pretreatment with rapamycin, on insulin-induced 2-DOG uptake after chronic insulin treatment Since insulin-stimulated phosphorylation of Akt and PKCλ activity decreased by the chronic insulin treatment was ameliorated by rapamycin treatment and expression of ΔIP-SHIP2 and IRS-1, we next examined these effects on insulin stimulation of 2-DOG uptake (Fig. 5a). Again, insulin-induced 2-DOG uptake was markedly decreased to 25.6±5.2% after chronic insulin treatment. Pretreatment with rapamycin and expression of ΔIP-SHIP2 partially restored the decreased 2-DOG uptake to 47.5±3.7% and 54.4±4.1%, respectively, of the control level. Both rapamycin treatment and ΔIP-SHIP2 expression more efficiently ameliorated the reduced 2-DOG uptake to 69.2±4.4%. Advanced overexpression of IRS-1 also improved the reduced 2-DOG uptake to 69.7 ±2.5% of the control level. The amount of Glut4 protein was not altered either by chronic insulin treatment, treatment with rapamycin, or overexpression of ΔIP-SHIP2 and IRS-1 (Fig. 5b).

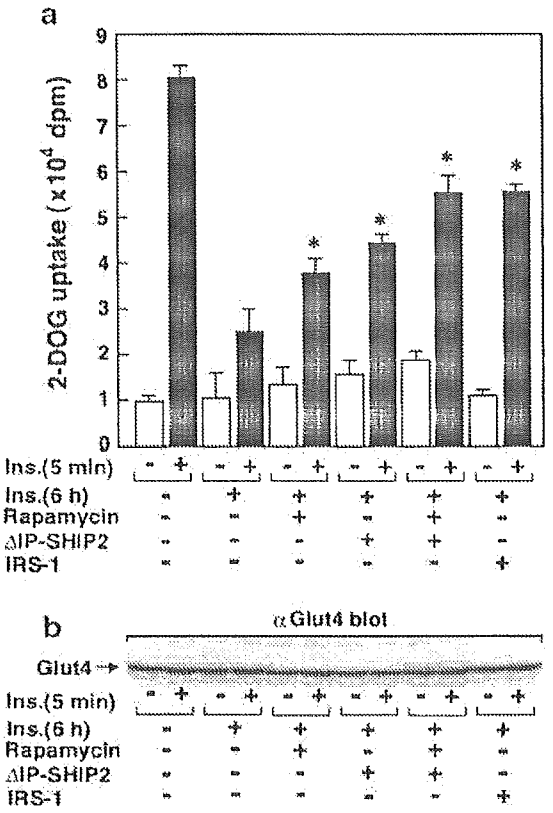

Fig. 5 Effect of ΔIP-SHIP2 and IRS-1 expression, and pretreatment with rapamycin, on insulin-induced 2-DOG uptake after chronic insulin treatment. 3T3-L1 adipocytes were transfected with LacZ and ΔIP-SHIP2 at an m.o.i. of 40 pfu/cell, or IRS-1 at an m.o.i. of 10 pfu/cell. Serum-starved transfected cells were incubated with vehicle or 20 nmol/l rapamycin for 30 min, and treated with 100 nmol/l insulin for 6 h. The cells were washed with PBS, incubated in insulin-free medium for 3 h, and washed again with PBS and incubated in glucose-free medium for another 30 min. After the cells had been stimulated with 10 nmol/l insulin for 5 min, 3.7 kBq of 2-[^{3}H]DOG was added for 3 min. The reaction was stopped by the addition of 10 μmol/l cytochalasin B. The cells were washed three times with PBS and solubilized with 0.2 mmol/l SDS–0.2 N NaOH. **a** The radioactivity incorporated into the cells was measured with a liquid scintillation counter. Results are means ± SEM of three separate experiments. *$p<0.05$ versus insulin-induced 2-DOG uptake in LacZ-transfected control cells with chronic insulin treatment. **b** The cell lysates were separated by SDS-PAGE and immunoblotted with anti-Glut4 antibody.

Discussion

Chronic insulin exposure is known to cause a subsequent insulin resistance, by reducing the level of IRS-1 via PI3-kinase and rapamycin-dependent pathways [17–21, 30, 31]. In fact, our results demonstrated that chronic insulin treatment induced a reduction in IRS-1 levels in a time-dependent manner. In addition to the impaired IRS-1–dependent signalling pathway, the present study showed increased amounts of SHIP2 following chronic insulin exposure. Since SHIP2 is the physiologically important negative regulator of insulin signalling with a fundamental impact on the state of insulin resistance [8–12], the increase in SHIP2 protein appears to be part of the novel molecular mechanism of insulin resistance caused by chronic insulin treatment. Because SHIP2 is translocated to the plasma membrane where it functions to hydrolyse PI(3,4,5)P3, the increase in the amount of SHIP2 protein in the plasma membrane preparation further supports the possible involvement of SHIP2 in insulin resistance in 3T3-L1 adipocytes [26].

We employed two approaches to ameliorate the decrease in IRS-1 levels caused by the chronic insulin treatment. As shown in Fig. 3, pretreatment with rapamycin prevented the mTOR-dependent proteosomal degradation of IRS-1 caused by the chronic insulin treatment. Overexpression of exogenous IRS-1 in advance normalized the decreased IRS-1 levels caused by the insulin treatment. On the other hand, endogenous SHIP2 function was efficiently inhibited by expression of the 5′-phosphatase defective dominant-negative SHIP2 (ΔIP-SHIP2) as shown in Fig. 2. These approaches would be useful for clarifying whether the rescue of insulin signalling at the level of IRS-1 and/or SHIP2 is effective in ameliorating insulin resistance caused by chronic insulin treatment. The decrease in the phosphorylation of Akt caused by the chronic insulin treatment was effectively ameliorated by either prevention of the decrease in IRS-1 by rapamycin treatment or advanced IRS-1 overexpression, or inhibition of endogenous SHIP2 function by expression of the dominant-negative SHIP2 (ΔIP-SHIP2). These results indicate that insulin-induced phosphorylation of Akt is closely associated with the IRS-1–mediated PI3-kinase pathway. In addition, the full input of insulin signal does not appear to be required for the sufficient phosphorylation of Akt, because amelioration of insulin signalling at the step involving IRS-1

or SHIP2 is sufficient for the efficient restoration of the phosphorylation of Akt.

Phosphorylation at both Thr^{308} and Ser^{473} is required for the full activation of Akt [8, 26–28]. In this context, our results showed that the rescue of IRS-1 levels by treatment with rapamycin and overexpression of IRS-1 in advance, and expression of the dominant-negative SHIP2 (ΔIP-SHIP2), efficiently ameliorated the decreased insulin-induced phosphorylation of Akt at both residues caused by the chronic insulin treatment. In contrast to the effective recovery of acute insulin stimulation of Akt phosphorylation, the recovery of acute insulin stimulation of PKCλ activation was only partial for both the restoration of IRS-1 levels and inhibition of SHIP2 function. Thus, pretreatment with rapamycin, advanced IRS-1 overexpression, and ΔIP-SHIP2 expression only partially ameliorated the insulin-induced activation of PKCλ to 49.8±3.8%, 67.2± 8.5%, and 65.0±7.5%, respectively, of the control value. The rescue of the PKCλ activity was still partial with a combination of ΔIP-SHIP2 expression and rapamycin pretreatment (or IRS-1 expression—data not shown). Therefore, the insulin resistance caused by chronic treatment may also impair insulin signalling at the step important for PKCλ activation more directly in addition to the IRS-1–PI3-kinase pathway. It is possible that another insulin signalling system important for glucose uptake including the CAP–Cbl–TC10 pathway may be a candidate implicated in the signalling step, although further investigation is needed to clarify the issue [32, 33]. We can not rule out the possibility that full activation of the IRS-1–PI3-kinase pathway is required for the efficient activation of PKCλ, although resistance at the levels of IRS-1 and SHIP2 appears to be efficiently rescued by pretreatment with rapamycin and expression of ΔIP-SHIP2.

Interestingly, the decreased stimulation of 2-DOG uptake caused by chronic insulin treatment was only partly restored by the maintenance of IRS-1 levels by pretreatment with rapamycin or advanced overexpression of IRS-1, or expression of ΔIP-SHIP2 as shown in Fig. 5. These findings are consistent with the results of PKCλ activation, and not Akt activation. Although Akt and atypical PKC are downstream effectors of PI3-kinase strongly implicated in the metabolic actions of insulin, the relative importance of Akt versus atypical PKC in insulin-induced 2-DOG uptake is controversial [8, 22, 27–29, 34]. Our results indicate that PKCλ/ζ rather than Akt may be more closely linked to the insulin-stimulated glucose uptake and associated with the state of insulin resistance. It is unclear whether this difference between Akt and PKCλ activation in chronic insulin treatment reflects a small input of IRS-1–dependent insulin signalling sufficient for Akt activation, or whether factors other than IRS-1–dependent insulin signalling are involved in the impairment of PKCλ activation. In any event, our results indicate that PKCλ activity rather than Akt activity appears to be associated with the decreased glucose uptake caused by chronic insulin treatment. Regardless of the importance of PKCλ to the state of insulin resistance, overexpression of the constitutively active form of PKCλ did not completely rescue the decreased insulin-stimulated glucose uptake caused by the chronic insulin treatment (data not shown). Based on this observation, chronic insulin treatment appears to cause insulin resistance at multiple signalling steps including a step distal to the PKCλ activation leading to the glucose uptake. It is also possible that chronic insulin treatment impairs the glucose uptake involved in the Glut4 translocation system independent of insulin signalling as previously reported for the insulin resistance caused by dexamethasone treatment in 3T3-L1 adipocytes [23].

In summary, SHIP2 appears to participate in insulin resistance, at least in part, caused by chronic insulin treatment in 3T3-L1 adipocytes. In addition, (1) impaired early insulin signalling occurring mainly at IRS-1 for the PI3-kinase activation, (2) impaired insulin signalling for PKCλ activation, and (3) impaired glucose transport system may also be involved in the insulin resistance caused by chronic insulin treatment. Furthermore, the present study indicates that the inhibition of endogenous SHIP2 appears to be effective at ameliorating the insulin signal in a state of insulin resistance, and that the activity of PKCλ rather than Akt may be more closely associated with the decreased 2-DOG uptake caused by the chronic insulin treatment in 3T3-L1 adipocytes. Taken together, inhibition of the endogenous level and/or function of SHIP2 would be an important therapeutic target of insulin resistance in type 2 diabetes.

Acknowledgements This work was supported in part by a grant-in-aid for scientific research from the Japan Society for the Promotion of Science. We thank Dr Wataru Ogawa (Kobe University, Japan) for kindly providing the anti-PKCλ antibody and Dr Kazuyuki Hiratani (Toyama Medical and Pharmaceutical University, Japan) for technical assistance. T. Sasaoka and K. Fukui contributed equally to this work.

References

1. Rameh LE, Cantley LC (1999) The role of phosphoinositide 3-kinase lipid products in cell function. J Biol Chem 274:8347–8350
2. Cantley LC (2002) The phosphoinositide 3-kinase pathway. Science 296:1655–1657
3. Virkamäki A, Ueki K, Kahn CR (1999) Protein–protein interaction in insulin signaling and the molecular mechanisms of insulin resistance. J Clin Invest 103:931–943
4. Czech MP, Corvera S (1999) Signaling mechanisms that regulate glucose transport. J Biol Chem 274:1865–1868
5. Saltiel AR, Pessin JE (2002) Insulin signaling pathways in time and space. Trends Cell Biol 12:65–71
6. Pesesse X, Deleu S, De Smedt F, Drayer L, Erneux C (1997) Identification of a second SH2-domain-containing protein closely related to the phosphatidylinositol polyphosphate 5-phosphatase SHIP. Biochem Biophys Res Commun 239:697–700
7. Ishihara H, Sasaoka T, Hori H et al (1999) Molecular cloning of rat SH2-containing inositol phosphatase 2 (SHIP2) and its role in the regulation of insulin signaling. Biochem Biophys Res Commun 260:265–272
8. Wada T, Sasaoka T, Funaki M et al (2001) Overexpression of SH2-containing inositol phosphatase 2 results in negative regulation of insulin-induced metabolic actions in 3T3-L1 adipocytes via its 5′-phosphatase catalytic activity. Mol Cell Biol 21:1633–1646

9. Sasaoka T, Hori H, Wada T et al (2001) SH2-containing inositol phosphatase 2 negatively regulates insulin-induced glycogen synthesis in L6 myotubes. Diabetologia 44:1258–1267
10. Clement S, Krause U, Desmedt F et al (2001) The lipid phosphatase SHIP2 controls insulin sensitivity. Nature 409:92–97
11. Hori H, Sasaoka T, Ishihara H et al (2002) Association of SH2-containing inositol phosphatase 2 with the insulin resistance of diabetic db/db mice. Diabetes 51:2387–2394
12. Marion E, Kaisaki PJ, Pouillon V et al (2002) The gene INPPL1, encoding the lipid phosphatase SHIP2, is a candidate for type 2 diabetes in rat and man. Diabetes 51:2012–2017
13. Reaven GM (1988) Role of insulin resistance in human disease. Diabetes 37:1595–1607
14. DeFronzo RA, Ferrannini E (1991) Insulin resistance: a multifaceted syndrome responsible for NIDDM, obesity, hypertension, dyslipidemia, and atherosclerotic cardiovascular disease. Diabetes Care 14:173–194
15. Goalstone ML, Natarajan R, Standley PR et al (1998) Insulin potentiates platelet-derived growth factor action in vascular smooth muscle cells. Endocrinology 139:4067–4072
16. Rondinone CM, Wang L-M, Lonnroth P, Wesslau C, Pierce JH, Smith U (1997) Insulin receptor substrate (IRS) 1 is reduced and IRS-2 is the main docking protein for phosphatidylinositol 3-kinase in adipocytes from subjects with non-insulin-dependent diabetes mellitus. Proc Natl Acad Sci U S A 94:4171–4175
17. Ricort J-M, Tanti J-F, Van Obberghen E, Le Marchand-Brustel Y (1995) Alterations in insulin signalling pathway induced by prolonged insulin treatment of 3T3-L1 adipocytes. Diabetologia 38:1148–1156
18. Thomson MJ, Williams MG, Frost SC (1997) Development of insulin resistance in 3T3-L1 adipocytes. J Biol Chem 272: 7759–7764
19. Berg CE, Lavan BE, Rondinone CM (2002) Rapamycin partially prevents insulin resistance induced by chronic insulin treatment. Biochem Biophys Res Commun 293:1021–1027
20. Haruta T, Uno T, Kawahara J et al (2000) A rapamycin-sensitive pathway down-regulates insulin signaling via phosphorylation and proteasomal degradation of insulin receptor substrate-1. Mol Endocrinol 14:783–794
21. Takano A, Usui I, Haruta T et al (2001) Mammalian target of rapamycin pathway regulates insulin signaling via subcellular redistribution of insulin receptor substrate 1 and integrates nutritional signals and metabolic signals of insulin. Mol Cell Biol 21:5050–5062
22. Kotani K, Ogawa W, Matsumoto M et al (1998) Requirement of atypical protein kinase Cλ for insulin stimulation of glucose uptake but not for Akt activation in 3T3-L1 adipocytes. Mol Cell Biol 18:6971–6982
23. Sakoda H, Ogihara T, Anai M et al (2000) Dexamethazone-induced insulin resistance in 3T3-L1 adipocytes is due to inhibition of glucose transport rather than insulin signal transduction. Diabetes 49:1700–1708
24. Sun XJ, Goldberg JL, Qiao L, Mitchell JJ (2002) Insulin-induced insulin receptor substrate-1 degradation is mediated by the proteasome degradation pathway. Diabetes 48:1359–1364
25. Zhande R, Mitchell JJ, Wu J, Sun XJ (2002) Molecular mechanism of insulin-induced degradation of insulin receptor substrate 1. Mol Cell Biol 22:1016–1026
26. Ishihara H, Sasaoka T, Ishiki M et al (2002) Membrane localization of src homology 2-containing inositol 5′-phosphatase 2 via Shc association is required for the negative regulation of insulin signaling in rat1 fibroblasts overexpressing insulin receptors. Mol Endocrinol 16:2371–2381
27. Kitamura T, Ogawa W, Sakaue H et al (1998) Requirement for activation of the serine-threonine kinase Akt (protein kinase B) in insulin stimulation of protein synthesis but not of glucose transport. Mol Cell Biol 18:3708–3717
28. Wang Q, Somwar R, Bilan PJ et al (1999) Protein kinase B/Akt participates in Glut4 translocation by insulin in L6 myoblasts. Mol Cell Biol 19:4008–4018
29. Bandyopadhyay G, Standaert ML, Zhao L et al (1997) Activation of protein kinase C (α, β, and ζ) by insulin in 3T3/L1 cells: transfection studies suggest a role for PKC-ζ in glucose transport. J Biol Chem 272:2551–2558
30. Pessin JE, Saltiel AR (2000) Signaling pathways in insulin action: molecular targets of insulin resistance. J Clin Invest 106:165–169
31. Sykiotis GP, Papavassiliou AG (2001) Serine phosphorylation of insulin receptor substrate-1: a novel target for the reversal of insulin resistance. Mol Endocrinol 15:1864–1869
32. Baumann CA, Ribon V, Kanzaki M et al (2000) CAP defines a second signalling pathway required for insulin-stimulated glucose transport. Nature 407:202–207
33. Chiang S-H, Baumann CA, Kanzaki M et al (2001) Insulin-stimulated Glut4 translocation requires the CAP-dependent activation of TC10. Nature 410:944–948
34. Bandyopadhyay G, Kanoh Y, Sajan MP, Standaert ML, Farese RV (2000) Effects of adenoviral gene transfer of wild-type, constitutively active, and kinase-defective protein kinase C-λ on insulin-stimulated glucose transport in L6 myotubes. Endocrinology 141:4120–4127

nature cell biology

Stat3-induced apoptosis requires a molecular switch in PI(3)K subunit composition

Kathrine Abell[1], Antonio Bilancio[2], Richard W. E. Clarkson[1], Paul G. Tiffen[1], Anton I. Altaparmakov[1], Thomas G. Burdon[3], Tomoichiro Asano[4], Bart Vanhaesebroeck[2,5] and Christine J. Watson[1,6]

Physiological apoptosis is induced by a switch from survival to death signalling. Dysregulation of this process is frequently associated with cancer[1]. A powerful model for this apoptotic switch is mammary gland involution, during which redundant milk-producing epithelial cells undergo apoptosis[2]. Signal transducer and activator of transcription 3 (Stat3) is an essential mediator of this switch but the mechanism has not yet been defined[3]. Stat3-dependent cell death during involution can be blocked by activation of Akt/protein kinase B (PKB)[4], a downstream effector of the phosphoinositide-3-OH kinase (PI(3)K) pathway[5]. Here we show that expression of the PI(3)K regulatory subunits p55α and p50α is induced by Stat3 during involution. In the absence of Stat3 *in vivo*, upregulation of p55α and p50α is abrogated, levels of activated Akt are sustained and apoptosis is prevented. Chromatin immunoprecipitation assays show that Stat3 binds directly to the p55α and p50α promoters *in vivo*. Overexpression of either p55α or p50α reduces levels of activated Akt. We propose a novel mechanism in which Stat3 regulates apoptosis by inducing expression of distinct PI(3)K regulatory subunits to downregulate PI(3)K-Akt-mediated survival signalling.

Stats are a family of latent transcription factors that mediate signalling from cytokines and growth factors[6]. Using conditional gene targeting, we have previously shown that activation of Stat3 is essential for the early phase of mammary gland involution because deletion of Stat3 resulted in reduced levels of apoptosis and delayed post-lactational regression[3]. Recently we found leukaemia inhibitory factor (LIF) to be the physiological activator of Stat3 *in vivo*[7], but so far the downstream effectors of this Stat3-dependent apoptotic signal have not been defined. Identification of these downstream effectors is important because constitutive Stat activity is often associated with tumorigenesis[8].

Involution is characterized by extensive apoptosis of the epithelial cells and a dramatic switch from survival to death signalling[2]. This apoptotic switch is exemplified in Fig. 1 showing that in involution the activity of the anti-apoptotic kinase Akt/PKB, as measured by its phosphorylation on Ser473, is downregulated (Fig. 1a, b) whereas Stat3 is activated (Fig. 1b). This change correlates with the induction of cell death as measured by a TdT-mediated dUTP nick end labelling (TUNEL) assay (Fig. 1a) and cleaved caspase-3 immunoblotting (Fig. 1b). Akt/PKB is activated in a PI(3)K-dependent manner[5] and negatively regulated by the tumour suppressor PTEN[9]. Transgenic expression of constitutively active mutants of Akt/PKB inhibit the induction of mammary epithelial cell death[4], thus overriding the pro-apoptotic signal from Stat3. It is therefore important for Akt/PKB to be downregulated in order to shift the balance in favour of the pro-apoptotic effects of Stat3.

To determine the mechanism by which Akt/PKB is downregulated at the apoptotic switch, we examined the expression level of PTEN, by western blot analysis (Fig. 1b). Surprisingly, the protein level of PTEN is also substantially reduced in involution, indicating that PTEN is unlikely to be the mechanism of phospho-Akt/PKB (pAkt/PKB) downregulation. We therefore measured the activity of PI(3)K across the lactation–involution transition (Fig. 1c) and found that pan-p85-associated PI(3)K activity was reduced threefold in involution compared with lactation. This provides an explanation for the low levels of pAkt/PKB in involution.

The reciprocal activation of Stat3 and Akt/PKB at the apoptotic switch prompted us to investigate whether there is any cross-talk between these death and survival pathways, by using tissue from mammary glands that are deficient in Stat3. Figure 1d shows that the level of pAkt/PKB and Akt/PKB is high in lactating control mice and that both forms are downregulated at the onset of involution. In contrast, pAkt/PKB activity was sustained in involuting Stat3-deficient mammary glands whereas total levels of Akt/PKB were diminished. We can conclude that Stat3 is a negative regulator of pAkt/PKB, but not total Akt/PKB, and that the levels of pAkt/PKB and Akt/PKB are regulated independently (Fig. 1d).

This intriguing observation prompted us to investigate the possible mechanism for this cross-talk between the Stat3 and PI(3)K-Akt/PKB pathways. The class IA PI(3)Ks are heterodimeric enzymes composed

[1]Mammary Apoptosis and Development Group, Department of Pathology, Tennis Court Road, University of Cambridge, Cambridge CB2 1QP, UK. [2]Cell Signalling Laboratory, Ludwig Institute for Cancer Research, London W1W 7BS, UK. [3]Roslin Institute, Roslin, Midlothian, EH25 9PS, UK. [4]Third Department of Internal Medicine, Faculty of Medicine, University of Tokyo, Tokyo 113, Japan. [5]Department of Biochemistry and Molecular Biology, University College London, Gower Street, London WC1E 6BT, UK.
[6]Correspondence should be addressed to C.J.W. (e-mail: cjw53@mole.bio.cam.ac.uk)

Published online: 27 March 2005; DOI: 10.1038/ncb1242

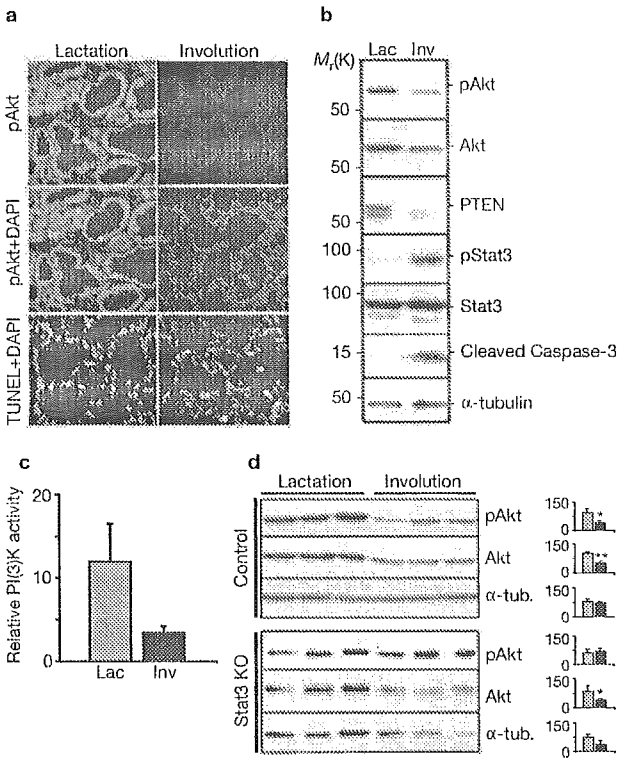

Figure 1 Activity of PI(3)K-Akt and Stat3 pathways during the apoptotic switch in mammary glands. (a–c) Mammary glands harvested at 10 day lactation (Lac) and 2 day involution (Inv) were analysed for (a) phospho-Ser 473-Akt/PKB (pAkt; green) and TUNEL staining (green) by immunoflourescence of paraffin sections. Blue or red indicate nuclei. (b) Akt/PKB and pAkt/PKB, PTEN, Stat3 and phospho-Stat3 (Tyr 701), and cleaved caspase-3 by immunoblotting and (c) pan-p85 antibody-associated PI(3)K activity. (d) Akt/PKB and pAkt/PKB as determined by immunoblot in glands from control or Stat3-deficient (Stat3 KO) glands. Each lane denotes one individual mouse. Graphs in c and d show mean ± s.d. Grey bars represent lactation, black bars represent involution. Asterisks denote statistical significance (*$P<0.05$; **$P<0.01$) in a two-tailed Student's *t*-test comparing 10-day lactation with 2-day involution. In b and d, α-tubulin was used as loading control.

of a regulatory subunit (p85α, p85β, p55α, p55γ or p50α)[10–15] and a p110 catalytic subunit (p110α, p110β or p110δ)[16,17]. Whereas p85β and p55γ are encoded by distinct genes, p85α, p55α and p50α are believed to be alternative splice forms of a single gene, *pik3r1* (refs 14, 15). Structurally, p85α, p55α and p50α share a common carboxy-terminal domain (Fig. 2a). In contrast, their amino termini are unique sequences of 340 amino acids (aa) (p85α), 34 aa (p55α) and 6 aa (p50α), respectively. It has been shown that changes in the regulatory subunit expression level can result in substantial changes in PI(3)K signalling[15,18–20]. We therefore speculated that alteration in the subunit composition of PI(3)K may be responsible for the reduced PI(3)K activity and hence the drop in pAkt/PKB during the apoptotic switch.

To investigate this hypothesis, we examined the expression of the PI(3)K regulatory subunits p85α, p85β, p55α, p55γ and p50α throughout mammary gland development, by western blot analysis using both a pan-p85 antibody and subunit-specific antibodies (Fig. 2b). The protein level of p55α was upregulated eightfold at the onset of involution, coinciding with epithelial cell apoptosis and activation of Stat3. The expression of the p50α subunit also increased during involution. In contrast, the full-length subunit p85α was substantially downregulated at the onset of involution, in a similar pattern to p85β. The expression of p55γ was constant throughout the developmental time course.

To investigate whether this marked and reciprocal expression of the three *pik3r1* splice forms p85α, p55α and p50α was occurring at the transcriptional level, we measured the levels of the individual transcripts using real-time PCR (Fig. 2c). Expression levels of p55α and p50α were upregulated approximately threefold and fivefold, respectively, by 12 h of involution. In contrast, the transcription of p85α was downregulated twofold within 24 h. This indicates that the downregulation of the p85α protein is due to transcriptional regulation and not proteolytic degradation.

Given the marked regulation of the regulatory subunits, it was important to determine whether any of the catalytic subunits were differentially expressed at the apoptotic switch. However, in contrast to the regulatory subunits, the expression of the three class IA catalytic subunits was unchanged at this time (Fig. 2d).

Thus, there is a distinct switch in the expression profile of the regulatory subunits with a marked transcriptional upregulation of p55α and p50α and downregulation of p85α, whereas the expression of p55γ and the three catalytic subunits is constant during the apoptotic switch. We have found that p55α interacts directly with p110α, p110β and p110δ (data not shown). This suggests that inducing the expression of the p55α and p50α subunits may be the means by which PI(3)K activity is regulated.

The striking correlation between the expression of the p55α and p50α subunits and the activation of Stat3 prompted us to investigate whether there is a direct connection between Stat3 activity and the induction of these two regulatory subunits. Therefore, we examined the expression of p85α, p55α and p50α in Stat3-deficient mammary glands from involuting mice (Fig. 3a). The protein levels of p55α and p50α were both significantly reduced in Stat3-deficient glands compared with controls (p55α, twofold; p50α, fourfold). In contrast, there was no significant change in the protein levels of p85α. Thus, Stat3 selectively upregulates the expression of p55α and p50α subunits in involution.

This was confirmed in tissue from LIF-deficient animals (Fig. 3b). The levels of p55α and p50α were significantly reduced in the LIF knockout mice compared with control, whereas no significant change was observed in the levels of p85α. Because the pan-p85 antibody used in these studies detects both p55α and p55γ, the levels of these subunits were determined individually. The expression of p55γ was unaltered whereas there was a significant reduction of p55α levels in LIF knockout mice. Taken together, this indicates the existence of a novel signalling pathway from LIF via Stat3 to p55α/p50α.

To examine whether Stat3 regulates the expression of p55α and p50α at the transcriptional level, we examined the mRNA level of the three *pik3r1*-encoded subunits by real-time PCR in lactating and involuting mice from Stat3-deficient and wild-type glands (Fig. 3c). *p55α* and *p50α* mRNAs were substantially upregulated in involution compared with lactation in control mice. In contrast, both *p55α* mRNA and *p50α* mRNA failed to be significantly upregulated in Stat3-deficient glands. Importantly, the levels of *p85α* mRNA were not significantly changed in the absence of Stat3.

We have previously shown that LIF-mediated activation of Stat3 induces apoptosis in a conditionally immortal mammary epithelial cell line (KIM-2)[7]. To investigate whether LIF/Stat3 could induce expression of the regulatory subunits in this cell line, we treated the cells with LIF and examined

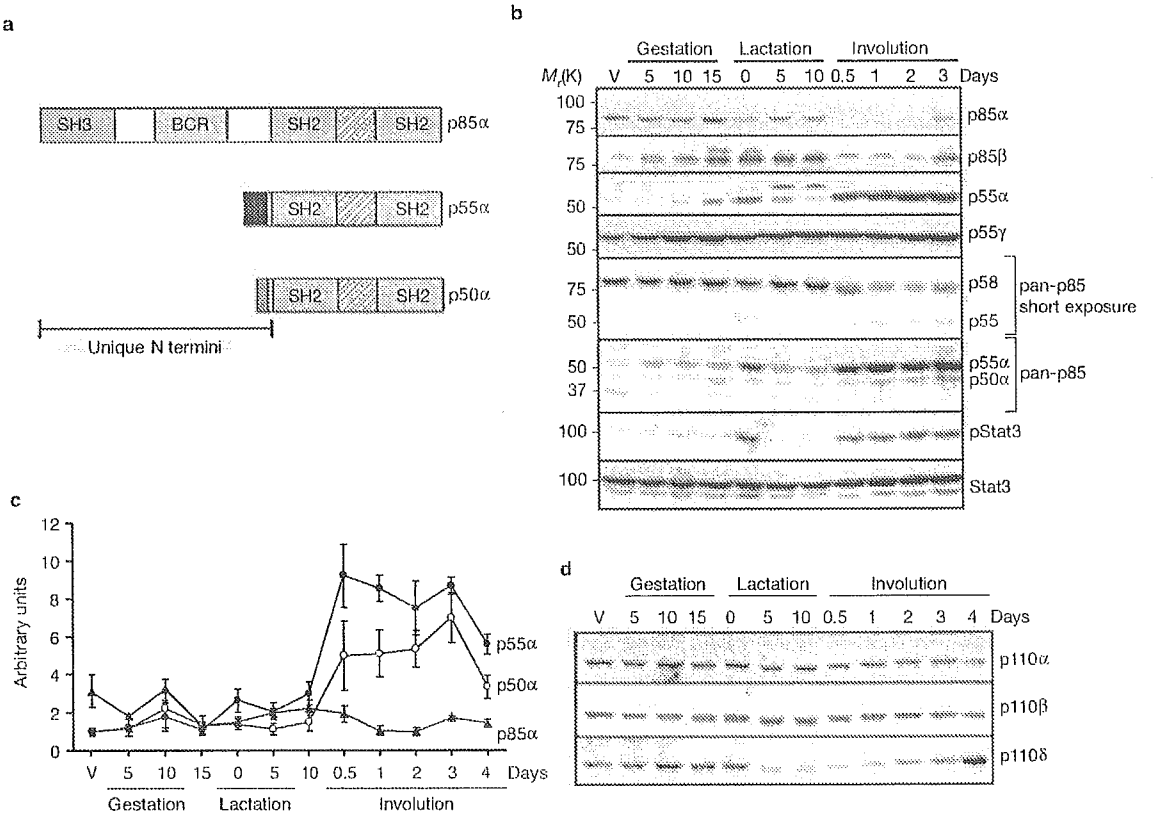

Figure 2 Differential expression of PI(3)K regulatory and catalytic subunits across the apoptotic switch. (a) Schematic drawing of the *pik3r1* splice forms. (b, d) Expression profiles across mammary gland development was determined by immunoblot using regulatory subunit specific antibodies (p85α, p85β, p55α, or p55γ), pan-p85 antibody (short and longer exposures) and antibodies against Stat3 and phospho-Stat3 (b) or catalytic subunit-specific antibodies (p110α, p110β or p110δ) (d). (c) Normalized gene expression of p85α, p55α and p50α across mammary gland development was determined by real-time PCR. Graph shows mean ± s.d. In b and c the results are representative of at least three mice per time point. V, virgin mammary gland tissue.

the expression of all three subunits by immunoblotting (Fig. 3d). A twofold upregulation of p55α and an eightfold upregulation of p50α were observed after 4 h treatment with LIF, whereas no significant change in the level of p85α was detected. This was associated with cleavage of caspase-3 after 24 h. Thus, the upregulation of p55α/p50α by LIF/Stat3 is specific to epithelial cells and coincides with induction of apoptosis.

To investigate whether p55α and p50α are direct transcriptional targets of Stat3, we used the mammary epithelial cell line KIM-2 expressing an inducible Stat3–gyrase fusion protein, which allows ligand-independent dimerization and activation of Stat3 in the presence of coumermycin[21] and is associated with the induction of mammary epithelial cell apoptosis (M. B. Boland, R.W.E.C., E. A. Kritikou, J. M. Lee, T. Freeman, P.G.T. and C.J.W., unpublished observations). Induced dimerization of the Stat3-gyrase fusion protein for only 4 h resulted in a significant increase in mRNA levels of *c-fos*, a known target of Stat3 (ref. 22), *p55α* and *p50α*, whereas levels of *p85α* mRNA were unchanged (Fig. 4a). This new identification of components of the PI(3)K pathway as downstream targets of the Jak/Stat pathway is tantalizing because it couples survival and death signalling directly. The specificity of this link is emphasized further by the finding that neither *p55α* nor *p50α* mRNA expression are induced by ligand-independent activation of the related Stat5 transcription factor (data not shown). Given this rapid induction of expression, we suggest that p55α and p50α but not p85α are direct transcriptional targets of Stat3 in epithelial cells.

The LIF/Stat3 pathway is essential for self-renewal of mouse embryonic stem (ES) cells[23]. LIF mediates its effects through activation of Stat3, extracellular-signal-related kinase (ERK) and PI(3)K[24]. The mechanism of PI(3)K-mediated survival signalling is not clear. However, disruption of the *pik3r1* gene in ES cells results in undetectable levels of all three *pik3r1*-encoded transcripts and increased levels of apoptosis[25]. To investigate whether Stat3 directly induces p55α/p50α expression in ES cells, we examined the mRNA levels of the three *pik3r1* gene products in ES cells expressing a chimeric receptor that consisted of the extracellular domain of granulocyte colony-stimulating factor (G-CSF) and the intracellular domain of gp130 with a mutation of the Tyr 118 to a phenylalanine (Fig. 4b). Treatment with G-CSF, which leads to specific hyper-activation of Stat3 (ref. 23), induced transcriptional upregulation of the Stat3-target suppressor of cytokine signalling 3 (Socs3), but not p85α, p55α nor p50α. This suggests that the Stat3-p55α/p50α pathway is selective to cell types in which Stat3 induces cell death.

The selective induction of p55α/p50α expression in response to Stat3 suggests that these transcripts may be transcribed from alternate promoter(s), and are not splicing isoforms. This prompted us to examine the genomic sequence of the *pi3kr1* locus. The genomic organization of the mouse *pik3r1* gene is shown in Fig. 5a. *p85α* mRNA is encoded by exon 1B and exons 2–18, *p50α* is encoded by exon 1C and exons 8–18. *p55α* is encoded by exon 1C and exons 8–18. Using *in silico* promoter

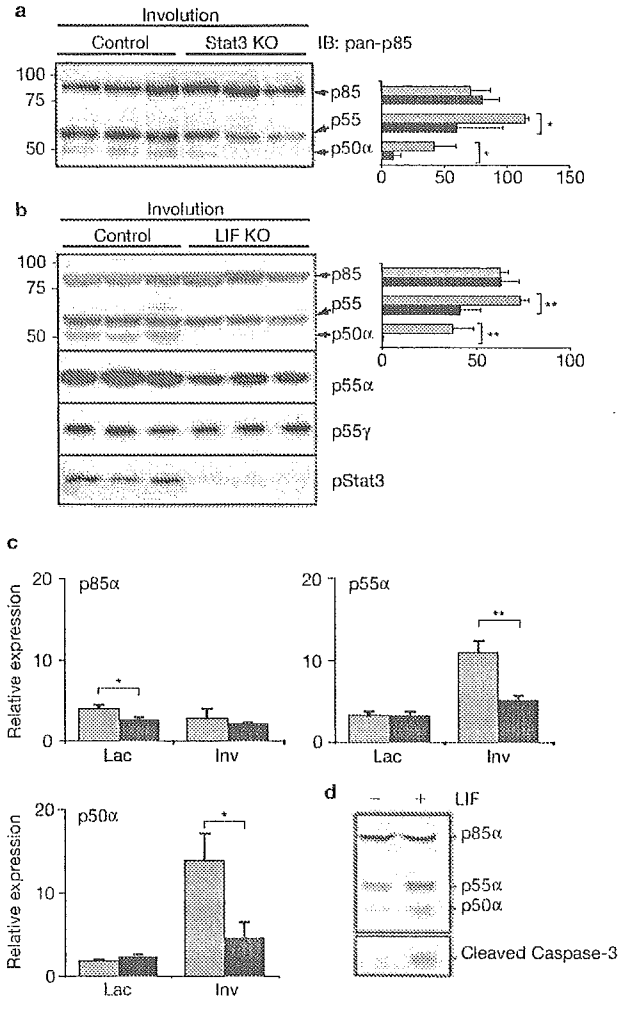

Figure 3 p55α and p50α are transcriptional targets of Stat3 *in vivo*. (**a**, **b**) p85, p55 and p50α protein expression determined by anti pan-p85 immunoblot in Stat3-knockout or anti-pan-85, anti-p55α and anti-p55γ immunoblot (**a**) and in LIF-knockout glands at 2 day involution (**b**). Each lane denotes one mouse. (**c**) Gene expression of p85α, p55α and p50α in Stat3-knockout glands from 10 day lactation and 2 day involution was determined by real-time PCR. Results are representative of at least three mice per time point. Real-time PCR results were normalized to cyclophilin mRNA. Graphs in **a**–**c** show means ± s.d. of control (grey) or test (black). Asterisks denote statistical significance (*$P<0.05$; **$P<0.01$) in a two-tailed Student's *t*-test comparing knockout to control glands. (**d**) Western blot analysis of p85, p55 and p50α expression and cleavage of caspase-3 in mammary epithelial KIM-2 cells treated with LIF for 4 h and 24 h, respectively.

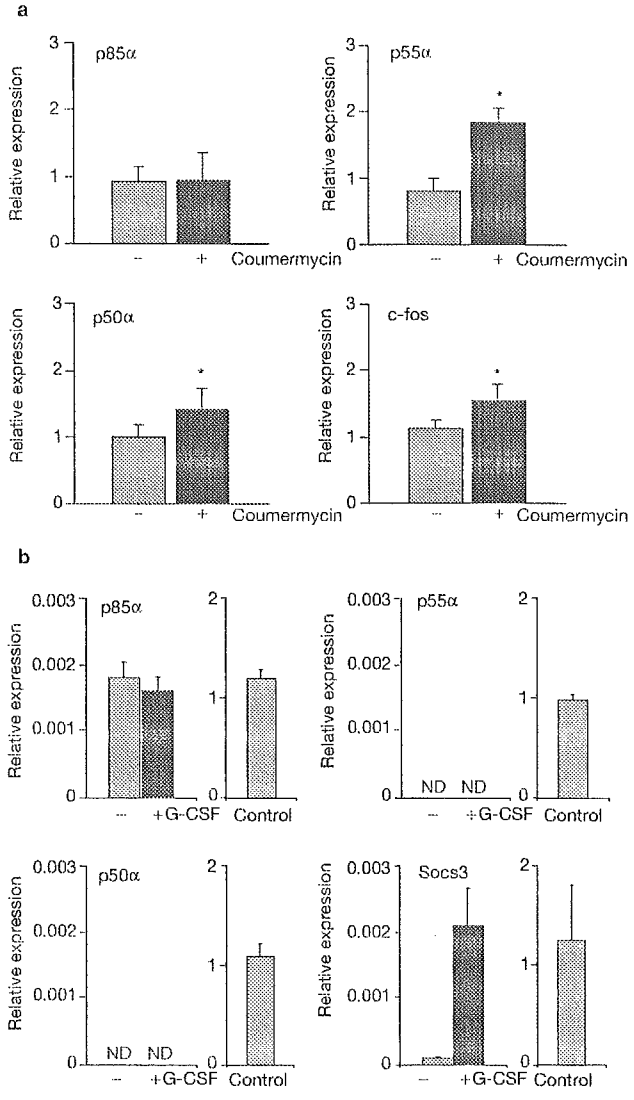

Figure 4 Stat3 regulates transcription of p55α and p50α in mammary, but not ES cells. (**a**) Transcription of p85α, p55α, p50α and c-fos in Stat3-GyrB-KIM-2 cells untreated (grey) or treated with coumermycin for 4 h (black) as determined by real-time PCR. (**b**) Gene expression of p85α, p55α, p50α and Socs3 in G-CSF-gp130-expressing ES cells untreated (grey) or treated with G-CSF for 1 h (black) as determined by real-time PCR. A pool of lactation and involution mammary gland cDNA was used as positive control. ND, not detectable. Real-time PCR results were normalized to cyclophilin mRNA. Graphs show means ± s.d. of control (grey) or test (black). Asterisks denote statistical significance (*$P<0.05$) in a two-tailed Student's *t*-test comparing treated versus untreated cells.

prediction tools, and information on 5′ cap sites, we have identified putative promoter regions 5′ flanking to exon 1A (p85α), 1B (p50α) and 1C (p55α), respectively. The potential p85α promoter contains a CpG island and several GC-boxes, and p50α a CpG island, whereas the potential p55α promoter contains a putative initiator consensus at the transcription start site. Potential Stat-binding motifs are present within the putative promoter regions of both p55α and p50α. To examine whether these Stat sites bind Stat3 *in vivo*, we performed chromatin immunoprecipitation (ChIP) assay in glands from lactating and involuting mice using promoter-specific primers and real-time PCR (Fig. 5b). The ChIP assay shows that Stat3 binds to the Stat consensus sequence in both the p50α and the p55α promoters *in vivo* in the involuting gland. Interestingly, Stat3 is associated with the promoter region of p50α in both lactation and involution. Because levels of unphosphorylated Stat3 are high in lactation (Fig. 1b), this indicates that the promoter region of p50α can be preloaded with inactive Stat3. Dynamic shuttling of unphosphorylated Stats 1, 2 and 3 is well documented and we have evidence of the presence of unphosphorylated Stat3 in nuclear extracts from lactating mammary gland (data not shown). We suggest that activation of Stat3 in involution by LIF results in the displacement of inactive Stat3 and transcriptional activation of p50α. In contrast, the p55α promoter only binds Stat3 in involution, providing

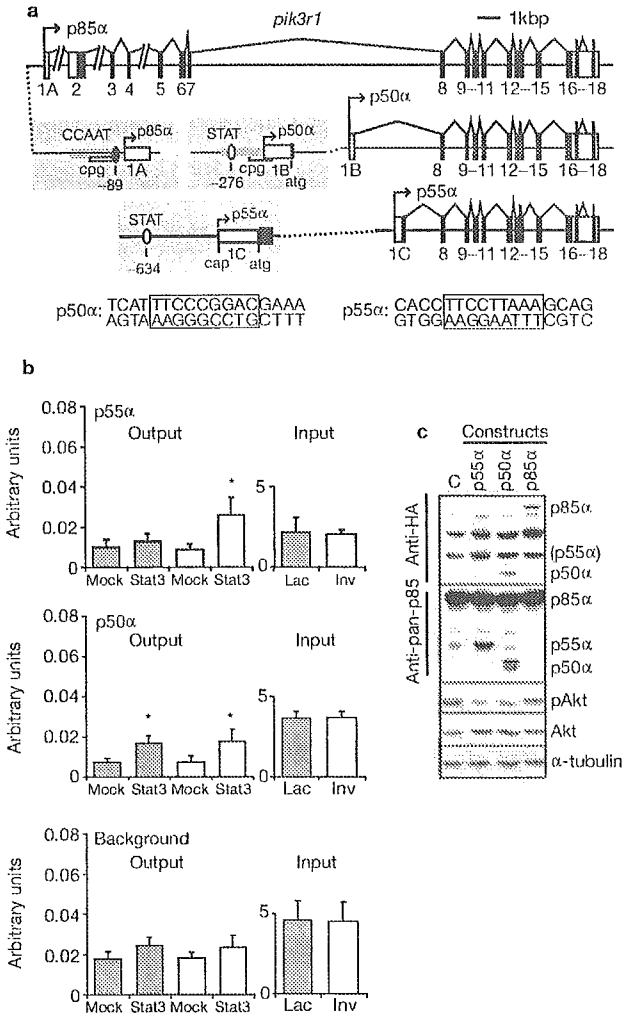

Figure 5 Expression of p55α and p50α is directly regulated by Stat3 *in vivo* and reduces levels of pAkt *in vitro*. (a) Genomic structure of *pik3r1* gene. The mouse *pik3r1* gene contains 20 exons spanning 84.76 kb. Intron 1 spans 9.9 kb and intron 2 47.8 kb. Boxes denote exons and filled boxes denote translated exons. Putative promoter regions are shown in enlarged format. Regions identified using PromoterInspector and FirstEF (p85α and p50α) are shown in grey boxes. The transcription start site for p55α was identified from the 5′ end of oligo-capped mRNA. (b) ChIP assays were performed on glands from lactating (grey) and involuting (white) mice using promoter-specific primers that span the Stat3-binding site and real-time PCR. The assay background was determined using primers directed against an upstream non-promoter sequence. Asterisks denote statistical significance (*$P<0.05$) in a two-tailed Student's *t*-test comparing isotype-matched control IgG (mock) with Stat3-specific antibody. Graphs show means ± s.d. of lactation (grey) or involution (white) timepoints. (c) Adenovirus-mediated over-expression of the p55α, p50α and p85α regulatory subunits in differentiated KIM-2 cells. Expression of the subunits was assessed by immunoblot with an antibody that recognizes the HA tag (upper panel) and the pan-p85 antibody (middle panel). The p55α is masked by an unspecific band in the HA immunoblot but is clearly visible with the pan-p85 antibody. Decreased levels of pAkt were detected in the extracts from the p55α and p50α over-expressing cells but not in the p85α over-expressing cells (bottom panel), whereas total Akt and α-tubulin levels were unchanged.

evidence that Stat3 binding to the p55α promoter is independent of Stat3 binding to the p50α promoter and is thus indisputably dependent on phosphorylation and activation of Stat3. We conclude that expression of the p85α, p50α and p55α transcripts from the *pik3r1* gene is regulated by distinct, subunit-specific promoters and that expression of p55α and p50α is regulated directly by Stat3.

Our results identify the two PI(3)K regulatory subunits p55α and p50α as direct transcriptional targets of Stat3 *in vivo* and show that upregulation of p55α and p50α is associated with reduced PI(3)K-Akt/PKB signalling. This was confirmed by over-expression of the three *pik3r1* subunits in fully differentiated mammary epithelial cells (Fig. 5c). These results show directly that expression of either p55α or p50α, but not p85α, results in diminished levels of pAkt/PKB. We propose, therefore, the existence of a previously unknown pro-apoptotic pathway by which Stat3 mediates a molecular switch in the subunit composition of PI(3)K, via activation of subunit-specific promoters, to downregulate Akt/PKB survival signalling, and suggest that this is a mechanism by which Stat3 exerts its pro-apoptotic function in mammary epithelial cells. This intriguing result provides an insight into the role of constitutively active Stat3 in carcinogenesis[8] and it will be interesting to determine whether dysregulated Stat3 mediates its oncogeneic effects by failing to induce the switch in PI(3)K subunit composition. Furthermore, in a mouse model of obesity and non-insulin-dependent diabetes mellitus, the *ob/ob* mouse, it has been shown that the levels of p55α and p50α subunits are elevated in liver[26]. Fatty livers from *ob/ob* mice are characterized by hyperactivation of Stat3 (ref. 27), and it is tempting to speculate that these two events are linked.

Taken together, these data strongly suggest that Stat3-mediated regulation of p55α and p50α determines the response of cells to environmental signals through modulating the activity of the PI(3)K-Akt/PKB pathway. □

METHODS

Generation of mice and tissues. The generation and genotyping of conditional Stat3 knockout mice and LIF-deficient mice has been described previously[17,28]. Mammary tissue was collected from $Stat3^{-/-}$, $Stat3^{+/+}$, $LIF^{-/-}$ and $LIF^{+/+}$ and wild-type mice after 10 days of lactation and 2 days following forced involution, initiated by removal of the pups after 10 days of lactation. All animals were killed by cervical dislocation. Whole abdominal mammary glands were removed followed by excision of lymph nodes and were snap-frozen in liquid nitrogen for protein or RNA extraction. For sectioning, whole glands were fixed in formalin and embedded in paraffin.

Cell culture and transfection. The mouse mammary epithelial cell line KIM-2 was established and cultured as described previously[7]. The Stat3-GyrB construct subcloned into pMX-puro for retroviral transduction was generated by M. Farrar and kindly provided by A. Mui (University of British Columbia, Canada). The generation of Stat3- and Stat5-GyrB pMX-puro constructs were generated as described[22] and stably introduced into KIM-2 cells. ES cells were cultured as described[23] and the gp130 mutant ES cells were generated as described[23]. KIM-2 cells were treated with LIF (50 ng ml^{-1}) for either 4 or 24 h and cells were collected for immunoblotting as described below.

Adenovirus-mediated expression of PI(3)K regulatory subunits. Adenoviral constructs and supernatants were prepared as described previously[20]. KIM-2 cells were differentiated for 12 days with differentiation media (DMEM/F12 containing 10% FCS and the lactogenic hormones prolactin, dexamethasone and insulin) as previously described[7] and infected with recombinant adenovirus encoding haemagglutinin (HA)-tagged p50α, p55α or p85α subunit sequences in the presence of differentiation media. Cells were collected 18 h post-infection and processed for immunoblotting as described below.

Immunoblotting. Lymph node-free abdominal mammary glands and cells were extracted with a lysis buffer containing 50 mM Tris-HCl pH 7.4, 1% NP-40, 0.25% Na-deoxycholate, 150 mM NaCl, 1 mM EDTA, 1 mM PMSF, 1 μg ml^{-1} aprotinin,

1 μg ml^{-1} leupeptin, 1 μg ml^{-1} pepstatin, 20 μg ml^{-1} bestatin, 20 μM TPCK, 1 mM Na_3VO_4, 1 mM NaF, 5 mM $Na_4P_2O_7$ as described previously[7]. Protein concentration was determined with the BCA colorimetric assay (Pierce, Rockford, IL) and immunoblotting and antibody detection using enhanced chemiluminescence (ECL, Amersham pharmacia biotech, Piscataway, NJ) were performed using standard procedures. The following rabbit antibodies from Cell Signaling Technology (Beverly, MA) were used: anti-pAkt/PKB (Ser 473), anti-total Akt/PKB, anti-PTEN, anti-cleaved caspase-3 and anti-phospho-Stat3 (Tyr 701). Other commercial antibodies used were mouse anti-stat3 (Transduction Laboratories, Lexington, KY), rat anti-α-tubulin (Abcam, Cambridge, UK), rabbit anti-HA tag (Santa Cruz Biotechnology, Santa Cruz, CA) and a rabbit anti-pan-p85 (Upstate Biotechnology, Lake Placid, NY). The anti-pan-p85 antibody recognizes the p85α, p55α and p50α isoforms, and cross-reacts weakly with p85β and p55γ (ref. 19; data not shown). The class IA regulatory subunit-specific antibodies were directed against the unique N termini of the p85α, p85β, p55α and p55γ, respectively, as described[13,15]. The p55γ antibody recognizes both p55γ and an additional protein of similar molecular weight (data not shown). The generation of isoform-selective antibodies to p110α, p110β and p110δ have been described previously[29]. Secondary HRP-conjugated antibodies were from Dako Cytomation, Glostrup, Denmark.

PI(3)K assay and immunoprecipitation. Proteins (500 μg) from lymph node-free abdominal mammary glands were immunoprecipitated using pan-p85 antibodies or non-immune control antibodies (rabbit anti-mouse IgG), and immunocomplex kinase assays were performed with PtdIns-4,5-bisphosphate as substrate essentially as described[29]. The phospholipids were resolved by thin-layer chromatography and radioactivity was quantified on Molecular Imager FX (Bio-Rad, Hercules, CA). The number indicate the radioactivity in the PtdIns-3,4,5-trisphosphate spot after subtraction of the radioactivity in a non-immune control precipitate, expressed as arbitrary PhosphorImager units.

Immunofluorescence and TUNEL assay. Immunofluorescene was performed using immunohistochemistry-specific rabbit-anti pAkt/PKB (Ser 473) antibodies (Cell Signaling Technology) and secondary Alexa Flour 488 goat anti-rabbit antibodies (Molecular probes, Eugene, OR) according to the supplier's instructions. TUNEL staining of paraffin-embedded sections was performed using ApopTag (Serological Corporation, Norcross, GA) according to the manufacturer's recommendations. Stained slides were mounted in Vectashield containing DAPI (Vector Labs, Burlingame, NH) and photographed under an inverted epi-fluorescence microscope (Leica, Bannockburn, IL).

RNA analysis. Total RNA was extracted from frozen tissue using the TRIzol reagent (Invitrogen, Paisley, UK) followed by additional column purification (Rneasy; Qiagen GmbH, Hilden, Germany). RNA integrity was monitored with Lab-on-a-chip 2100 Bioanalyzer (Agilent Technologies, Palo Alto, UK). cDNA was synthesized by random hexanucleotide-primed reverse transcription from 1 μg of total RNA using the Transcriptor reverse transcription cDNA synthesis kit (Roche, Basel, Switzerland). Quantitative detection of p85α, p55α, p50α, Socs3, and c-fos cDNA was performed using iCycler supermix (Bio-Rad) with the addition of flourescein and SYBR-green according to the supplier's recommendations. The real-time PCR reactions were run in an iCycler (Bio-Rad, Hercules, CA) in triplicate. The following forward and reverse primer pairs were used for specific amplification: p85α, 5′-GCC CCG TGC TTT TCA GAT TTC-3′, 5′-TCC TGC TGG TAT TTG GAC ACT GGG TAG-3′; p55α, 5′-GTT ACA GTG CGG GCC GTA TAG GTT TTA-3′, 5′-TCC TGC TGG TAT TTG GAC ACT GGG TAG-3′; p50α, 5′-CTG GCA GTT CAA AGC GAA ACC GT-3′, 5′-TCC TGC TGG TAT TTG GAC ACT GGG TAG-3′; SOCS-3, 5′-CCC GCG GGC ACC TTT CTT ATC-3′, 5′-TGC TTC GGG GGT CAC TCT GC-3′; c-fos, 5′-AGC GCA GAG CAT CGG CAG AAG-3′, 5′-GTT GAG AAG GGG CAG GGT GAA GG-3′; and cyclophilin, 5′-GACGCCACTGTCGCTTTTCG-3′, 5′-CTT GCCATCCAGCCATTCAGTC-3′. The expression values obtained were normalized against those obtained from control cyclophilin via a standard curve generated by serial dilution of pooled mammary gland cDNA.

Bioinformatics. The genomic organization of the mouse *pik3r1* gene was identified by mapping mRNA for p85α (GenBank accession number U50413), p55α (GenBank accession number AK046259) and p50α (GenBank accession number U50414) to the genomic sequence of mouse chromosome 13 (GenBank accession number AC107662) using BLAST (http://www.ncbi.nlm.nih.gov/blast/bl2seq/bl2.html) and the GenePalette software. One hundred kilobases (kb) of genomic sequence surrounding the *pik3r* gene were screened for the presence of potential promoter regions using PromoterInspector in the GenomatixSuite (http://www.Genomatix.de). Only sequences 5′-flanking exon 1A (p85α) and exon 1B (p50α) were identified as putative promoters in this region. These findings were confirmed using FirstEF[30]. The sequence encoding *p55α* mRNA (AK046259) was originally obtained by the oligo-capping method and the 5′ end of this sequence thus identifies the location of transcription initiation site and core promoter. CpG islands were identified using FirstEF and transcription factor binding sites by eye and by MatInspector (http://www.Genomatix.de).

Chromatin immunoprecipitation assay. ChIP assays were performed using the ChIP kit from Upstate Biotechnology (Lake Placid, NY) with the following modifications. Mammary glands from 10 day lactating and 2 day involuting mice were collected as described above, snap-frozen and ground into a powder under liquid nitrogen. The tissue was fixed in 1% formaldehyde/PBS supplemented with the Complete protease inhibitor cocktail (Roche Diagnostics, Basel, Switzerland), 1 mM Na_3VO_4 and 1 μg ml^{-1} pepstatin for 15 min at room temperature. Fixation was stopped by the addition of glycine to a final concentration of 125 mM. After several washes in ice-cold PBS, the tissue pellet was resuspended in NEBA buffer (10 mM HEPES, 10 mM KCl, 0.1 mM EDTA, 0.1 mM EGTA) supplemented with Complete protease inhibitor cocktail, 1 mM Na_3VO_4 and 1 μg ml^{-1} pepstatin, dounce homogenized and incubated for 15 min on ice. NP40 (0.5%) was added and samples were vortexed for 30 s before collecting the nuclei. Subsequently, the nuclear fraction was lysed in nuclear lysis buffer (50 mM Tris-HCl pH 8.1, 10 mM EDTA, 1% SDS, Complete protease inhibitor cocktail, 1 mM vanadate and 1 μg ml^{-1} pepstatin). Chromatin was sheared by sonication to a size of approximately 500 base pairs (bp), and samples were precleared for 2 h at 4 °C with salmon-sperm DNA–saturated protein-A/G Sepharose. Chromatin solutions were precipitated overnight at 4 °C with 2 μg of anti-Stat3 antibody (sc-482, Santa Cruz Biotechnology) or 2 μg of isotype-matched control IgG (Dako Cytomation). Immune complexes were collected with salmon-sperm DNA– saturated protein-A/G Sepharose for 3 h and were washed extensively following the manufacturer's protocol. Input and immunoprecipitated chromatin were incubated at 65 °C overnight with 0.3 M NaCl and 30 μg RNAse to reverse crosslinks. After proteinase K digestion, DNA was extracted with phenol and chloroform and was ethanol precipitated with 20 μg glycogen as carrier. Input and bound DNA was detected quantitatively by real-time PCR as described above using specific primers to amplify a 297 bp region (−244 to −541) spanning the Stat-binding site (−276) in the mouse p50α promoter and specific primers to amplify a 260 bp region (−375 to −635) spanning the Stat-binding site (−624) in the mouse p55α promoter. Assay background was determined using primers (−7130 to −7282 from p50α transcription start site) to amplify a product of 146 bp. The sequences of the PCR primers used are as follows: p50α, 5′-GTG GCC GAG GCA AGA CTA AC-3′, 5′-CTG CGG GGC TGA CTG TG-3′; p55α, 5′-ATC AGA TAT CCC AAG GTC AAA ACA AGA-3′, 5′-ACC TTC CTT AAA GCA GCT AGC AAT GAG-3′; background, 5′-GGC CAC TCA TCA GCT CTC ACC CAT AC-3′, 5′-GCT CTC TCA AGC CTC CAG CAA AAA CC-3′. Arbitrary concentrations of the amplified products were determined against a serial dilution of genomic DNA.

BIND identifiers. One BIND identifier (www.bind.ca) is associated with this manuscript: 217739.

Note: Supplementary Information is available on the Nature Cell Biology website.

ACKNOWLEDGEMENTS

This work was supported by BBSRC grant number G18086. A.B. was supported by the Ludwig Institute for Cancer Research and by FIRB 2001 (Italy). We thank P. Came and F. Baxter for providing the TUNEL data, T. Rich and B. Kedjouar for critical reading of the manuscript, D. Vetrie for advice on ChIP assay, and A. Tolkovsky and C. Goemans for help with the adenovirus assays.

COMPETING FINANCIAL INTERESTS

The authors declare that they have no competing financial interests.

Received 25 November 2004; accepted 25 February 2005
Published online at http://www.nature.com/naturecellbiology.

1. Schulze-Bergkamen, H. & Krammer, P. H. Apoptosis in cancer-implications for therapy. *Semin. Oncol.* **31,** 90–119 (2004).
2. Kumar, R., Vadlamudi, R. K. & Adam, L. Apoptosis in mammary gland and cancer. *Endocr. Relat. Cancer* **7,** 257–269 (2000).
3. Chapman, R. S. *et al.* Suppression of epithelial apoptosis and delayed mammary gland involution in mice with a conditional knockout of Stat3. *Genes Dev.* **13,** 2604–2616 (1999).
4. Schwertfeger, K. L., Richert, M. M. & Anderson, S. M. Mammary gland involution is delayed by activated Akt in transgenic mice. *Mol. Endocrinol.* **15,** 867–881 (2001).
5. Franke, T. F. *et al.* The protein kinase encoded by the Akt proto-oncogene is a target of the PDGF-activated phosphatidylinositol 3-kinase. *Cell* **2,** 727–736 (1995).
6. Levy, D. E. & Darnell, J. E. Jr. Stats: transcriptional control and biological impact. *Nature Rev. Mol. Cell Biol.* **3,** 651–662 (2002).
7. Kritikou, E. A. *et al.* A dual, non-redundant, role for LIF as a regulator of development and STAT3-mediated cell death in mammary gland. *Development* **130,** 3459–3468 (2003).
8. Yu, H. & Jove, R. The STATs of cancer - new molecular targets come of age. *Nature Rev. Cancer* **4,** 97–105 (2004).
9. Stambolic, V. *et al.* Negative regulation of PKB/Akt-dependent cell survival by the tumor suppressor PTEN. *Cell* **95,** 29–39 (1998).
10. Otsu, M. *et al.* Characterization of two 85 kd proteins that associate with receptor tyrosine kinases, middle-T/pp60c-src complexes, and PI3-kinase. *Cell* **65,** 91–104 (1991).
11. Pons, S. *et al.* The structure and function of p55PIK reveal a new regulatory subunit for phosphatidylinositol 3-kinase. *Mol. Cell Biol.* **15,** 4453–4465 (1995).
12. Antonetti, D. A., Algenstaedt, P. & Kahn, C. R. Insulin receptor substrate 1 binds two novel splice variants of the regulatory subunit of phosphatidylinositol 3-kinase in muscle and brain. *Mol. Cell Biol.* **16,** 2195–2203 (1996).
13. Inukai, K. *et al.* A novel 55-kDa regulatory subunit for phosphatidylinositol 3-kinase structurally similar to p55PIK is generated by alternative splicing of the p85 gene. *J. Biol. Chem.* **271,** 5317–5320 (1996).
14. Fruman, D. A., Cantley, L. C. & Carpenter, C. L. Structural organization and alternative splicing of the murine phosphoinositide 3-kinase p85 alpha gene. *Genomics* **37,** 113–121 (1996).
15. Inukai, K. *et al.* p85 gene generates three isoforms of regulatory subunit for phosphatidylinositol 3-kinase (PI 3-Kinase), p50, p55, and p85, with different PI 3-kinase activity elevating responses to insulin. *J. Biol. Chem.* **272,** 7873–7882 (1997).
16. Vanhaesebroeck, B., Leevers, S. J., Panayotou, G. & Waterfield, M. D. Phosphoinositide 3-kinases: a conserved family of signal transducers. *Trends Biochem. Sci.* **22,** 267–272 (1997).
17. Cantley, L. C. The phosphoinositide 3-kinase pathway. *Science* **296,** 1655–1657 (2002).
18. Ueki, K., Algenstaedt, P., Mauvais-Jarvis, F. & Kahn, C. R. Positive and negative regulation of phosphoinositide 3-kinase-dependent signaling pathways by three different gene products of the p85 regulatory subunit. *Mol. Cell Biol.* **20,** 8035–8046 (2000).
19. Ueki, K. *et al.* Molecular balance between the regulatory and catalytic subunits of phosphoinositide 3-kinase regulates cell signaling and survival. *Mol. Cell Biol.* **22,** 965–977 (2002).
20. Inukai, K. *et al.* Five isoforms of the phosphatidylinositol 3-kinase regulatory subunit exhibit different associations with receptor tyrosine kinases and their tyrosine phosphorylations. *FEBS Lett.* **490,** 32–38 (2001).
21. O'Farrell, A. M., Liu, Y., Moore, K. W. & Mui, A. L. IL-10 inhibits macrophage activation and proliferation by distinct signaling mechanisms: evidence for Stat3-dependent and -independent pathways. *EMBO J.* **16,** 1006–1018 (1998).
22. Leaman, D. W. *et al.* Roles of JAKs in activation of STATs and stimulation of c-fos gene expression by epidermal growth factor. *Mol. Cell Biol.* **16,** 369–375 (1996).
23. Niwa, H., Burdon, T., Chambers, I. & Smith, A. Self-renewal of pluripotent embryonic stem cells is mediated via activation of STAT3. *Genes Dev.* **12,** 2048–2060 (1998).
24. Burdon, T., Smith, A. & Savatier, P. Signalling, cell cycle and pluripotency in embryonic stem cells. *Trends Cell Biol.* **12,** 432–438 (2002).
25. Hallmann, D. *et al.* Altered signaling and cell cycle regulation in embryonal stem cells with a disruption of the gene for phosphoinositide 3-kinase regulatory subunit p85. *J. Biol. Chem.* **278,** 5099–5108 (2003).
26. Kerouz, N. J., Horsch, D., Pons, S. & Kahn, C. R. Differential regulation of insulin receptor substrates-1 and -2 (IRS-1 and IRS-2) and phosphatidylinositol 3-kinase isoforms in liver and muscle of the obese diabetic (*ob/ob*) mouse. *J. Clin. Invest.* **100,** 3164–3172 (1997).
27. Torbenson, M. *et al.* STAT-3 overexpression and p21 up-regulation accompany impaired regeneration of fatty livers. *Am. J. Pathol.* **161,** 155–161 (2002).
28. Dani, C. *et al.* Paracrine induction of stem cell renewal by LIF-deficient cells: a new ES cell regulatory pathway. *Dev. Biol.* **203,** 149–162 (1998).
29. Vanhaesebroeck, B. *et al.* Distinct PI(3)Ks mediate mitogenic signalling and cell migration in macrophages. *Nature Cell Biol.* **1,** 69–71 (1999).
30. Davuluri, R. V., Grosse, I. & Zhang, M. Q. Computational identification of promoters and first exons in the human genome. *Nature Genet.* **4,** 412–417 (2001). Erratum in *Nature Genet.* **3,** 459 (2002).

Am J Physiol Endocrinol Metab 289: E474–E481, 2005.
First published May 10, 2005; doi:10.1152/ajpendo.00003.2005.

Glycogen debranching enzyme association with β-subunit regulates AMP-activated protein kinase activity

Hideyuki Sakoda,[1] Midori Fujishiro,[1] Junko Fujio,[1] Nobuhiro Shojima,[1] Takehide Ogihara,[2] Akifumi Kushiyama,[1] Yasushi Fukushima,[1] Motonobu Anai,[3] Hiraku Ono,[3] Masatoshi Kikuchi,[3] Nanao Horike,[4] Amelia Y. I. Viana,[4] Yasunobu Uchijima,[4] Hiroki Kurihara,[4] and Tomoichiro Asano[4]

[2]Division of Advanced Therapeutics for Metabolic Diseases, Center for Translational and Advanced Animal Research on Human Diseases, Tohoku University Graduate School of Medicine, Sendai; [1]Department of Internal Medicine, Graduate School of Medicine; [3]Institute for Adult Disease, Asahi Life Foundation; and [4]Department of Physiological Chemistry and Metabolism, Graduate School of Medicine, University of Tokyo, Tokyo, Japan

Submitted 4 January 2005; accepted in final form 28 April 2005

Sakoda, Hideyuki, Midori Fujishiro, Junko Fujio, Nobuhiro Shojima, Takehide Ogihara, Akifumi Kushiyama, Yasushi Fukushima, Motonobu Anai, Hiraku Ono, Masatoshi Kikuchi, Nanao Horike, Amelia Y. I. Viana, Yasunobu Uchijima, Hiroki Kurihara, and Tomoichiro Asano. Glycogen debranching enzyme association with β-subunit regulates AMP-activated protein kinase activity. *Am J Physiol Endocrinol Metab* 289: E474–E481, 2005. First published May 10, 2005; doi:10.1152/ajpendo.00003.2005.—AMP-activated protein kinase (AMPK) regulates both glycogen and lipid metabolism functioning as an intracellular energy sensor. In this study, we identified a 160-kDa protein in mouse skeletal muscle lysate by using a glutathione-*S*-transferase (GST)-AMPK fusion protein pull-down assay. Mass spectrometry and a Mascot search revealed this protein to be a glycogen debranching enzyme (GDE). The association between AMPK and GDE was observed not only in the overexpression system but also endogenously. Next, we showed the β1-subunit of AMPK to be responsible for the association with GDE. Furthermore, experiments using deletion mutants of the β1-subunit of AMPK revealed amino acids 68–123 of the β1-subunit to be sufficient for GDE binding. W100G and K128Q, both β1-subunit mutants, are reportedly incapable of binding to glycogen, but both bound GDE, indicating that the association between AMPK and GDE does not involve glycogen. Rather, the AMPK-GDE association is likely to be direct. Overexpression of amino acids 68–123 of the β1-subunit inhibited the association between endogenous AMPK and GDE. Although GDE activity was unaffected, basal phosphorylation and kinase activity of AMPK, as well as phosphorylation of acetyl-CoA carboxylase, were significantly increased. Thus it is likely that the AMPK-GDE association is a novel mechanism regulating AMPK activity and the resultant fatty acid oxidation and glucose uptake.

glutathione-*S* transferase; pull-down assay; mass spectrometry

AMP-ACTIVATED PROTEIN KINASE (AMPK) acts as an intracellular energy sensor and regulates both glycogen and lipid metabolism (1–3). An increased intracellular AMP-to-ATP ratio leads to a conformational change in AMPK; AMPK is then phosphorylated and activated by LKB1. Activated AMPK reportedly phosphorylates and inactivates acetyl-CoA carboxylase (ACC) and decreases in malonyl-CoA, which increases fatty acid oxidation. 3-Hydroxy-3-methylglutaryl coenzyme A (HMG-CoA) reductase is also downregulated by AMPK, and cholesterol synthesis is thereby decreased. In skeletal muscle, contraction and 5-aminoimidazole-4-carboxamide-1-β-D-ribofuranoside (AICAR) stimulation increase AMPK activity and thereby increase GLUT4 translocation and glucose uptake (4). In addition, expression of GLUT4 protein is increased by continuous AICAR stimulation (5, 6), although events downstream from AMPK involving translocation and gene transcription of GLUT4 have not yet been clarified.

Energy storage in cells depends mainly on glycogen and lipid. Recently, it was reported that a considerable amount of AMPK colocalizes with glycogen particles. This has been attributed to the β-subunit of AMPK that contains a glycogen-binding domain (7–9). Although the physiological significance of this localization of AMPK with glycogen particles remains unclear, glycogen synthase was reported to be phosphorylated and deactivated by AMPK in vitro (10). In the skeletal muscle of AMPKα2 knockout mice, basal glycogen synthase activity is increased, and AICAR treatment fails to deactivate glycogen synthase (11). In addition, it was reported that the activation of AMPKα2 is increasingly suppressed as glycogen levels rise (12). Mutation of the AMPK γ-subunit reportedly increase glycogen content in skeletal muscle and the heart (13, 14). Thus AMPK has a close relationship, not only locationally but also functionally, with glycogen.

In this study, we attempted to identify proteins that bind to AMPK by using a glutathione-*S*-transferase (GST)-AMPK fusion protein pull-down assay, and found GDE to be the AMPK-associated protein. Herein, we show that GDE associates with AMPK and thereby modulates its kinase activity.

MATERIALS AND METHODS

Antibodies. The antibodies against the α- and β-subunits of AMPK and GDE were prepared by immunization of rabbits with a GSTα2 subunit, GSTβ1 subunit, and GDE fusion protein, respectively. These antibodies were then affinity purified as previously described (15). Anti-Flag, anti-hyaluronic acid (HA), and anti-c-myc antibody were purchased from Sigma; anti-AMPKβ, anti-phospho-AMPKα-Thr^{172}, and anti-phospho-ACC-Ser^{79} were purchased from Cell Signaling Technology; and anti-AMPKα1-specific antibody and anti-AMPKα2-specific antibody were purchased from Upstate Biotechnology.

Animals. Six-week-old male C57/BL6 mice and Sprague-Dawley rats were purchased from Tokyo Experimental Animals (Tokyo, Japan) and fed a standard rodent diet. Some mice were starved for

Address for reprint requests and other correspondence: Department of Physiological Chemistry and Metabolism, Graduate School of Medicine, University of Tokyo, 7-3-1 Hongo Bunkyo-ku, Tokyo, Japan (e-mail: asano-tky@umin.ac.jp).

The costs of publication of this article were defrayed in part by the payment of page charges. The article must therefore be hereby marked "*advertisement*" in accordance with 18 U.S.C. Section 1734 solely to indicate this fact.

12 h; these mice were then anesthetized with pentobarbital sodium (60 mg/kg body wt inositol 1,4,5-trisphosphate), and lower limb skeletal muscles were dissected out. The study protocol was approved by the Institutional Review Board of the Institute for Adult Disease, Asahi Life Foundation. Animal care was in accordance with the policies of the University of Tokyo at all times.

Cell culture. COS-7 cells and HEK293 cells were maintained in DMEM supplemented with 5% fetal bovine serum under a 5% CO_2 atmosphere at 37°C. Sf9 cells were maintained in Grace's medium supplemented with 5% fetal bovine serum at 27°C.

DNA constructs. cDNAs encoding human GDE and the β1-subunit of human AMPK were produced by PCR with primers corresponding to sequences already reported, using the cDNA library from HEK293 cells. All GDE and AMPKβ1 constructs were designed to contain a Flag or HA tag at the COOH terminus. Human AMPKα1, -α2, -β2, -γ1, and -γ2 cDNAs were kindly provided by Japan Tobacco, Central Pharmaceutical Research Institute (Osaka, Japan). W100G and K128Q, both β1-subunit mutants, were produced by PCR as reported previously (8). Fragments of the NH_2-terminal portion (amino acids 1–67), glycogen binding domain (GBD); (amino acids 68–163), and COOH- terminal portion (amino acids 164–270) of the β1-subunit were amplified by PCR with sense primers attached to the *Bam*HI site and a start codon: 5′-GGA TCC ATG GGC AAT ACC AGC AGT-3′, 5′-GGA TCC ATG GAA GTG AAT GAT AAA GCT-3′, or 5′-GGA TCC ATG GAT GCT TTA ATG GTG GA-3′, respectively, and with antisense primers attached to the HA tag and a stop codon: 5′-TCA AGC GTA GTC TGG GAC GTC GTA TGG GTA CAG ATC ATG CTG CCA GGC-3′, 5′-TCA AGC GTA GTC TGG GAC GTC GTA TGG GTA AAA TAC TTC AAA GTC-3′, or 5′-TCA AGC GTA GTC TGG GAC GTC GTA TGG GTA TAT GGG CTT GTA TAA-3′, respectively. The cDNAs encoding amino acids 68–113, 68–123, 68–133, 68–143, and 68–153 in the GBD of AMPKβ1 were amplified by PCR, with 5′-GGA TCC ATG GAA GTG AAT GAT AAA GCT-3′ as the sense primer and 5′-TCA AAA GTT ATT GTG GCT TCT-3′, 5′-TCA ATG CTC TCC TTC CGG-3′, 5′-TCA CCA CTG ACC ATC CAC-3′, 5′-TCA GGT TAC TAT GGG CTC-3′, and 5′-TCA AAT GAT GTT GTT AAC-3′ as antisense primers, respectively. The cDNA-encoding amino acids 113–163 of AMPKβ1 were amplified by PCR with 5′-GGA TCC ATG GTA GCC ATC CTG GAT CTG-3′ as the sense primer and 5′-TCA GTA AAA TAC TTC AAA GTC-3′ as the antisense primer. PCR products were cloned into a pCR2.1 plasmid vector (Invitrogen, San Diego, CA) and all sequences were confirmed using a CEQ2000 DNA Analysis System (Beckman Coulter).

Generation of recombinant adenovirus and baculovirus. Recombinant adenovirus used to express human GDE was constructed by homologous recombination of the expression cosmid cassettes containing the corresponding cDNAs and the parental virus genome, as described previously (16). The full-length coding regions of AMPKα2, including the GST sequence at the NH_2 terminus, AMPKβ1, AMPKγ2, and GDE in the pBacPAK9 transfer vector (Clontech), and the baculoviruses were prepared according to the manufacturer's instructions. For protein production, Sf9 cells were infected with these baculoviruses and grown for 48 h.

Purification of GST-AMPK fusion protein. GST and the GSTα2 subunit were overexpressed in Sf9 cells using baculoviruses and the cells were lysed with lysis buffer (PBS, 1% Triton X-100, 0.2 mmol/l PMSF). GST and the GSTα2 subunit fusion protein were isolated and purified by affinity chromatography on glutathione-Sepharose 4B (Pharmacia Biotech). The purified GST and GSTα2 subunit fusion protein were incubated with Sf-9 lysates of cells co-overexpressing the β1- and γ2-subunits of AMPK for 1 h and then washed six times with lysis buffer and used for the GST pull-down assay.

GST pull-down assay. Muscles were homogenized with 10 vol/wt homogenizing buffer [20 mmol/l Tris·HCl (pH 7.4), 1% Triton X-100, 0.25% sodium deoxycholate, 0.25 mol/l NaCl] containing 0.2 mmol/l PMSF and 5 μg/ml aprotinin and then centrifuged at 15,000 rpm for 30 min at 4°C. Next, the supernatants were recentrifuged at 100,000 *g* for 1 h. Then, 100 ml of supernatant (2 μg/ml protein concentration) were incubated with 1 ml of glutathione-Sepharose 4B for 1 h at 4°C to remove nonspecifically bound proteins, incubated with purified GST-AMPK fusion protein for 1 h, washed six times with homogenizing buffer, subjected to SDS-PAGE, and then silver stained. As a negative control, GST, preincubated only with Sf9 cells overexpressing the β1- and γ2-subunits, was incubated with tissue lysates from mouse skeletal muscle. GST-AMPK fusion protein not incubated with tissue lysates was also subjected to SDS-PAGE. The band specifically observed as an AMPK-associated protein was analyzed using mass spectrometry and Mascot search by Shimadzu Biotech (Ibaragi, Japan).

Purification of GST fusion protein and pull-down assay. cDNAs encoding full-length AMPKα2, AMPKβ1, and AMPKγ1 and fragments of the β1-subunit of AMPK were subcloned into a pGEX-4T-3 vector (Amersham Biosciences) that was used to transform *Escherichia coli* JM109. Transformed cells were grown to an A_{600} of 0.6 in LB medium supplemented with 0.1 mg/ml ampicillin and stimulated for 3 h with 1.0 mM isopropyl-β-D-1-thiogalactopyranoside. GST fusion proteins were isolated and purified by affinity chromatography on glutathione-Sepharose 4B (17). GDE-overexpressing Sf9 cell lysates were immunoprecipitated with anti-Flag M2-agarose (Sigma), and GDE was purified and eluted from the agarose with 3× Flag peptide (Sigma). Purified GDE was incubated with GST, GST containing full-length AMPKα2, AMPKβ1, or AMPKγ1, or various GST fragments of the β1-subunit of AMPK for 1 h. After six washes with lysis buffer, glutathione-Sepharose 4B beads were boiled in Laemmli buffer, followed by SDS-PAGE and Western blotting.

AMPK assay. After first serum-starving COS-7 cells for 2 h in serum-free DMEM, followed by preincubation for 1 h in Krebs-Ringer-HEPES buffer, the cells were stimulated with a 30-min incubation in Krebs-Ringer-HEPES buffer containing 2 mmol/l AICAR. Next, the COS-7 cells were lysed in *buffer A* and centrifuged. The supernatants were then immunoprecipitated with anti-AMPKα antibodies. AMPK activities in the immunoprecipitants were assayed using SAMS peptide, as described previously (15).

Glycogen debranching enzyme assay. After the serum starvation, preincubation, and AICAR stimulation previously described, COS-7 cells overexpressing GDE were collected with Tris buffer [20 mmol/l Tris·HCl (pH 7.5), 1 mmol/l sodium orthovanadate, 1 mmol/l β-glycerophosphate, and 0.2 mmol/l PMSF] and then sonicated. The sonicated cells were centrifuged at 17,000 *g* for 20 min, and the supernatants were immunoprecipitated with anti-Flag antibody. The immunoprecipitants were washed twice with Tris buffer and twice more with GDE assay buffer [20 mmol/l Tris·HCl (pH 7.5), 50 mmol/l sodium acetate]. Next, the immunoprecipitants were incubated at 37°C for 30 min in the GDE assay buffer containing 15 mmol/l glucosyl-β-cyclodextrin as the substrate (18–20), and GDE activities were determined by measuring the amount of glucose released from glucosyl-β-cyclodextrin, using the glucose oxidase method (GLU CII, Wako).

Immunopreciptation and immunoblotting. The supernatants from skeletal muscle and COS-7 cells, prepared as previously described, were immunoprecipitated with 3 μg/ml antibodies for 2 h. The immunoprecipitants were boiled in Laemmli sample buffer containing 100 mmol/l DTT and then subjected to SDS-PAGE and Western blotting with each antibody, as previously described. (21).

RESULTS

GST pull-down assay using GST-AMPK fusion protein-GST-AMPKα2 subunit fusion protein and the β- and γ-subunits were overexpressed in Sf9 cells using baculovirus. After the GSTα2-subunit had been purified with glutathione-Sepharose 4B, Sf9 cell lysates co-overexpressing the β1- and γ2-subunits of AMPK were added to the GST-α2-subunit bound

to glutathione-Sepharose 4B. Employing this procedure, a trimer consisting of α2-, β1-, and γ2-subunits was produced on glutathione-Sepharose 4B beads, although more than half of the α2-subunit was still not bound to the β1- and γ2-subunits. Next, purified GST-AMPK fusion proteins and GST alone were incubated with lysates from mouse skeletal muscle. GST-AMPK fusion and associated proteins were subjected to SDS-PAGE, followed by silver staining (Fig. 1*A*, *lane 2*). As a negative control, GST alone preincubated with β1- and γ2-subunits was incubated with tissue lysates from mouse skeletal muscle (Fig. 1*A*, *lane 1*). In *lane 3* of Fig. 1*A*, corresponding to the GST-AMPK fusion protein, three subunits and several bands derived from Sf9 cell lysates are apparent. A comparison with *lane 1*, corresponding to the GST-alone protein, revealed the 160-kDa single band in *lane 2* to be a protein binding specifically to AMPK. The 160-kDa band was trypsinized and analyzed using mass spectrometry and Mascot search. With the Mascot search method, protein scores exceeding 67 points are significant ($P < 0.05$). Five proteins had significant scores, and the highest, at 258 points, was rabbit GDE. The protein with the second highest score, 217 points, was rat GDE. Human GDE protein had a score of 174 points, the partial sequences of mouse GDE 94 and 75 points. All proteins with significant Mascot search results were GDEs, which consistently had very high scores. The identification of this 160-kDa protein as a GDE was confirmed with immunoblotting using anti-GDE antibody (data not shown). We thus concluded that the 160-kDa protein was, in fact, mouse GDE.

Subsequently, we examined the in vivo association between AMPKα and GDE. Mouse skeletal muscle lysates were immunoprecipitated with anti-AMPKβ antibody (Cell Signaling) or control IgG, and the immunoprecipitants were subjected to SDS-PAGE and immunoblotting using anti-GDE antibody. As shown in Fig. 1*B*, GDE was detected in the AMPKβ immunoprecipitant but not in the control IgG precipitant, which indicates a physiological association between AMPK and GDE. In addition, this association did not differ significantly, depending on whether the mice were fasted or fed.

GDE bound to the AMPKβ1-subunit directly. AMPK consists of a catalytic α-subunit and regulatory β- and γ-subunits. To examine which subunit binds GDE, each subunit and GDE were co-overexpressed in COS-7 cells and immunoprecipitated with each of the anti-tag antibodies. The α1-, α2-, β1-, and β2-subunits of AMPK were coimmunoprecipitated with GDE, whereas the γ1- and γ2-subunits were not (Fig. 2, *A*, *B*, and *C*). The 312 NH_2-terminal amino acid portion of the α-subunit does not bind to the β- and γ-subunits, since the association with the β-subunit is via the COOH-terminal portion of the α-subunit. The 312 NH_2-terminal amino acids of the α-subunit were found to not coimmunoprecipitate with GDE (Fig. 2*A*, *lower middle*). This raised the possibility that the coimmunoprecipitation of the α-subunit with GDE did not represent a direct association but rather binding with the β- or γ-subunit of AMPK.

To confirm that the β- but not the γ-subunit binds to GDE, GDE alone or GDE plus the β1-, β2-, γ1-, or γ2-subunit was overexpressed in COS-7 cells. In the GDE immunoprecipitant, the β1- and β2- but not the γ1- and γ2-subunits were detected (Fig. 2, *B* and *C*, *lower middle*). Similarly, GDE was detected

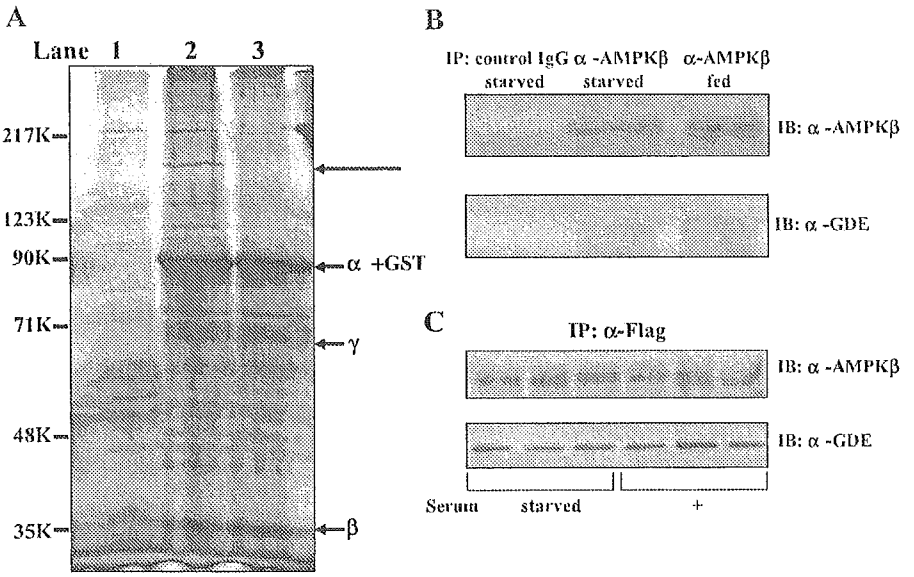

Fig. 1. Pull-down assays using glutathione-*S*-transferase-AMP-activated protein kinase (GST-AMPK) fusion proteins. *A*: GST and GST-AMPKα2 fusion proteins were overexpressed in Sf9 cells by using a baculovirus and then purified with glutathione-Sepharose 4B. Purified GST alone and GST-AMPKα2 fusion proteins were incubated with Sf9 cell lysates overexpressing AMPKβ1 and AMPKγ2 and then with a tissue lysate from mouse skeletal muscle for 1 h. Beads were washed 6 times with homogenizing buffer followed by SDS-PAGE and silver staining. *Lane 1*: GST alone was incubated with AMPKβ1 and AMPKγ2 and then with lysates from mouse skeletal muscle. *Lane 2*: GST-AMPKα2 was incubated with AMPKβ1 and AMPKγ2 and then with lysates from mouse skeletal muscle. *Lane 3*: GST-AMPKα2 was incubated with AMPKβ1 and AMPKγ2 but not with the mouse skeletal muscle lysate. A 160-kDa band (arrow, *lane 2*) was identified as glycogen debranching enzyme (GDE) by mass spectrometry and Mascot search technique. *B*: lysates from mouse skeletal muscle were immunoprecipitated (IP) with control IgG or anti-AMPKβ antibodies, followed by SDS-PAGE and Western blotting with anti-AMPKβ (*top*) or anti-GDE (*bottom*) antibodies. *C*: Flag-tagged GDE was overexpressed in COS-7 cells with adenoviruses. After being serum starved or not for 12 h, cells were lysed and immunoprecipitated with anti-Flag antibody. Immunoprecipitants were subjected to SDS-PAGE and Western blotting using anti-AMPKβ (*top*), and anti-GDE (*bottom*) antibodies.

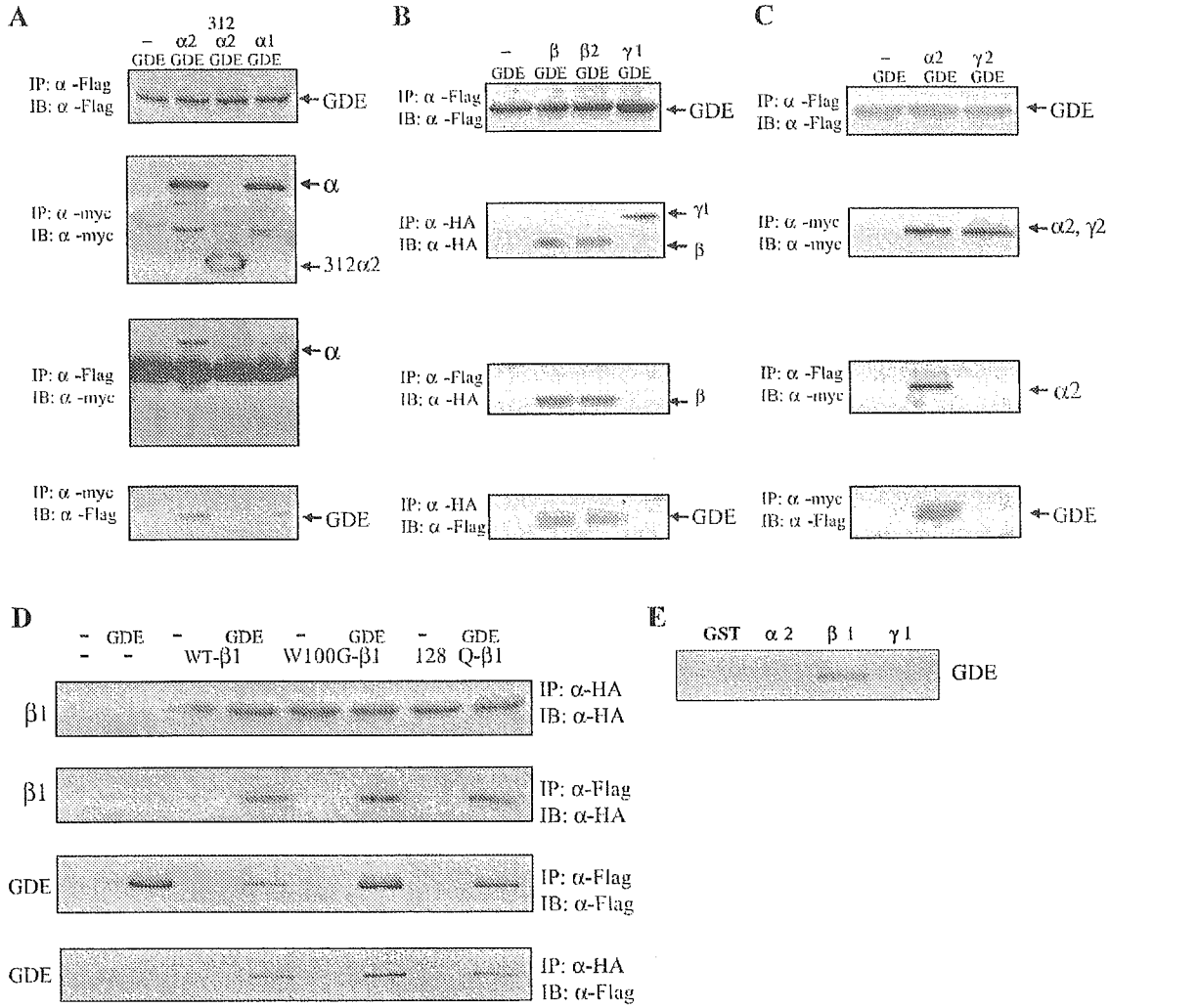

Fig. 2. β-Subunit of AMPK binds to GDE. *A*: GDE (Flag-tagged) and AMPKα2, 312 NH_2-terminal amino acids of AMPKα2, and -α1 (myc-tagged) were co-overexpressed in COS-7 cells. Cell lysates were immunoprecipitated with anti-myc or anti-Flag antibodies followed by SDS-PAGE and Western blotting (IB) with anti-myc or anti-Flag antibodies. *B*: GDE (Flag-tagged) and AMPKβ1, -β2 [(HA)-tagged], and AMPKγ1 (HA-tagged) were co-overexpressed in COS-7 cells. Cell lysates were immunoprecipitated with anti-HA or anti-Flag antibodies followed by SDS-PAGE and Western blotting with anti-HA or anti-Flag antibodies. *C*: GDE (Flag-tagged) and AMPKα2, and -γ2 (myc-tagged) were co-overexpressed in COS-7 cells. Cell lysates were immunoprecipitated with anti-myc or anti-Flag antibodies followed by SDS-PAGE and Western blotting with anti-myc or anti-Flag antibodies, respectively. *D*: GDE (Flag-tagged) and wild-type, W100G, and K128Q AMPKβ1 (HA-tagged) were overexpressed in Sf9 cells by baculoviruses. Cell lysates were immunoprecipitated with anti-HA or anti-Flag antibodies followed by SDS-PAGE and Western blotting with anti-HA or anti-Flag antibodies. *E*: GST fusion proteins containing full-length AMPKα2, -β1, or -γ1 were purified using glutathione-Sepharose 4B, as described in MATERIALS AND METHODS. GDE was purified using anti-FLAG M2-agarose (Sigma) and 3× Flag peptide (Sigma). Purified GDEs were incubated with GST, GST-AMPKα2, GST-AMPKβ1, or GST-AMPKγ1 for 1 h. After 6 washes with lysis buffer, glutathione-Sepharose 4B beads were boiled in Laemmli buffer followed by SDS-PAGE and Western blotting using anti-Flag antibody.

in the β1- and β2- but not the γ1- and γ2-subunit immunoprecipitants (Fig. 2, *B* and *C*, *bottom*).

In addition, pull-down assays were performed using GST-AMPK fusion protein with purified GDE. As shown in Fig. 2*E*, GDEs were pulled down by purified GST-AMPKβ1 fusion protein.

Thus we concluded that the β-subunit is responsible for the association of AMPK with GDE.

Recently, AMPKβ1 was reported to possess a glycogen binding domain (8, 9). GDE also binds to glycogen, and thus we speculate that AMPKβ1 and GDE coimmunoprecipitate through their glycogen binding domains rather than associating directly. To examine this possibility, β1-subunit mutants W100G and K128Q, both of which are incapable of binding glycogen (8), were overexpressed with or without GDE, as well as the wild-type β1-subunit (Fig. 2*D*). It was clearly demonstrated that these glycogen-binding, defective β1-subunit mutants still coimmunoprecipitate with GDE, just like the wild-type β1-subunit. This indicates that the association between the β-subunit and GDE does not involve glycogen but rather is direct.

GDE binding to an AMPK site. To identify the GDE binding site in the β1-subunit, we prepared various deletion mutants of the β1-subunit as GST fusion proteins (Fig. 3*A*). By use of these GST-AMPKβ1 fragment fusion proteins, pull-down assays were performed.

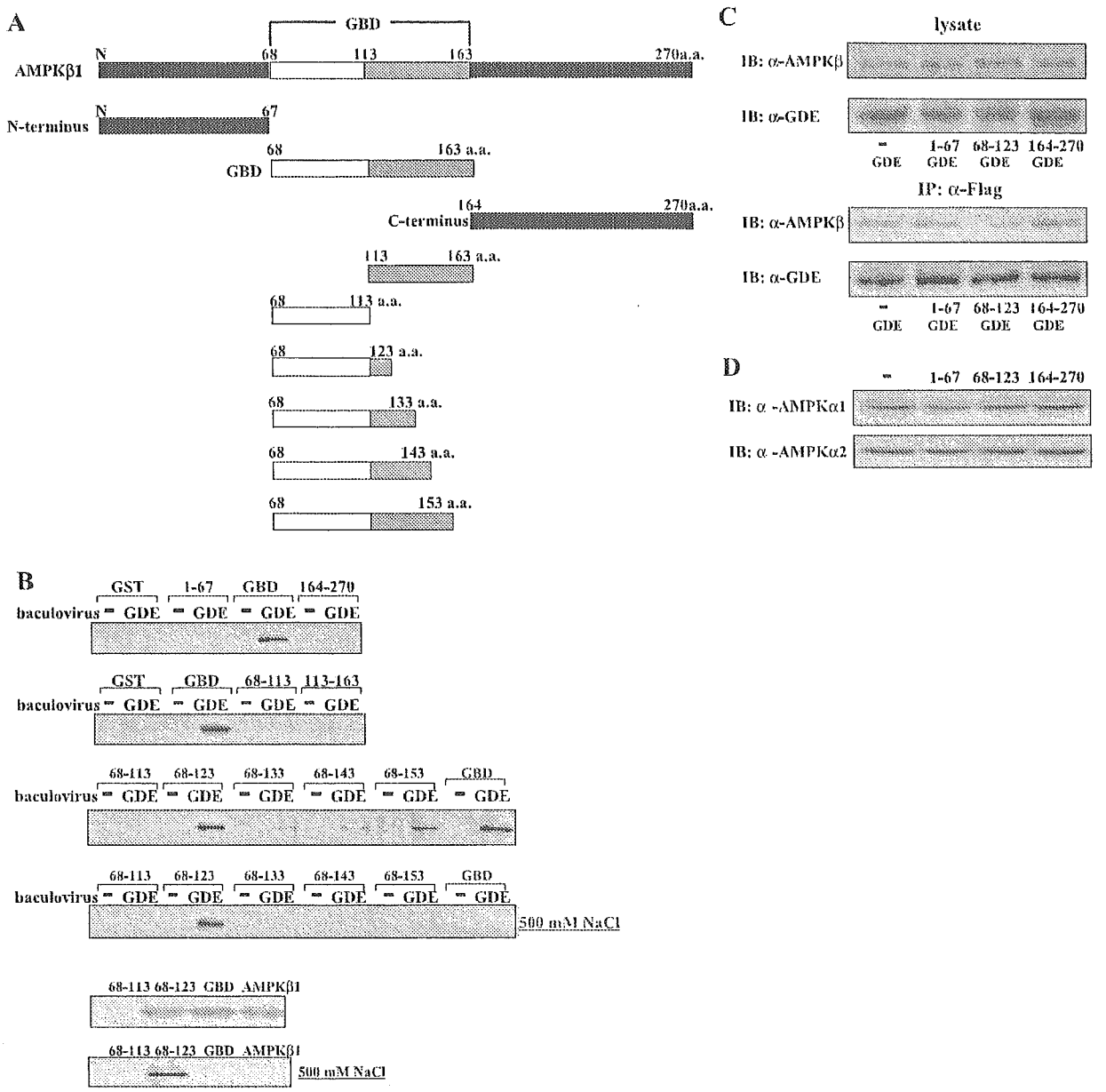

Fig. 3. Amino acids 68–123 of AMPKβ1 include the GDE binding site. *A*: schematic presentation of GST fragment of AMPKβ1 fusion protein. *B*: GST-AMPKβ1 fragment fusion proteins were overexpressed in JM109 and purified with glutathione-Sepharose 4B. Purified GST-AMPK fusion proteins were incubated with GDE (Flag-tagged) overexpressing Sf9 cell lysates for 1 h and then washed 6 times with lysis buffer followed by SDS-PAGE and Western blotting with anti-Flag antibody. The amino acids 68–123 sequence of the β1-subunit bound GDE most strongly. *C* and *D*: GDE and amino acids 1–67, 68–123, or 164–270 of the β1-subunit were overexpressed in COS-7 cells with adenoviruses. *C*: cells were lysed and immunoprecipitated with anti-Flag antibody. Immunoprecipitants were subjected to SDS-PAGE and Western blotting using anti-AMPKβ and anti-GDE antibodies. *D*: overexpression of amino acids 68–123 of the β1-subunit inhibited association of AMPKβ with GDE. Total cell lysates were subjected to SDS-PAGE and Western blotting using anti-AMPKα1- or -α2-specific antibody.

First, GST protein containing three fragments corresponding to the NH_2 terminus, GBD, and COOH terminus of the β1-subunit were purified with glutathione-Sepharose 4B, and the association with GDE was assessed by incubation with the lysate from GDE overexpressing Sf9 cells. Figure 3*B*, *panel 1*, shows clearly that the sequence responsible for the association with GDE is included in the GBD of the β1-subunit (Fig. 3*B*, *panel 1*). Next, GBD was separated into two fragments: amino acids 68–113 and amino acids 113–163 of the β1-subunit. However, we found that these fragments did not bind GDE (Fig. 3*B*, *panel 2*). Thus we prepared four additional β1-subunit deletion mutants of GBD: amino acids 68–123, 68–133, 68–143, and 68–153. Amino acids 68–123, but not 68–113, were demonstrated to be sufficient for binding with GDE (Fig. 3*B*, *panel 3*). Amino acid sequences 68–133 and 68–143 exhibited weaker binding with GDE than amino acids

68–123, although the reason for this is unclear. The binding of amino acids 68–123 with GDE was not abolished by washing with high-salt buffer (containing 500 mM NaCl), whereas those with full-length GBD and amino acid sequences 68–133, 68–143, or 68–153 were apparently reduced (Fig. 3*B*, *panel 4*). Thus it is likely that amino acids 68–123 of the β1-subunit possess a high affinity for GDE.

Inhibition of the association between GDE and AMPK increases AMPK activity. Amino acids 68–123 were used to inhibit the association between AMPK and GDE. Full-length GDE and amino acids 68–123 of the β1-subunit were overexpressed, and GDE was immunoprecipitated with anti-Flag antibody. As shown in Fig. 3*C*, overexpression of amino acids 68–123 of the β1-subunit inhibited the association between GDE and AMPKβ1, whereas the AMPKα1 and α2 protein expression levels were unchanged (Fig. 3*D*).

Under these conditions, we examined GDE or AMPK activities in COS-7 cells. Overexpressing amino acids 68–123 of the β1-subunit did not change GDE activities (Fig. 4*A*). On the other hand, basal AMPK activity increased significantly, by ~30%, compared with control cells (Fig. 4*B*). Basal phosphorylation of AMPKα-Thr^{172} was also increased by 35% (Fig. 4*C*). Phosphorylation of ACC-Ser^{79}, which is reportedly phosphorylated by AMPK, was also approximately doubled when amino acids 68–123 of the β1-subunit were overexpressed without AICAR stimulation (Fig. 4*D*). Thus it is very likely that inhibition of the association between GDE and AMPK increases AMPK activity.

DISCUSSION

AMPK is a regulator of the key enzymes involved in glucose and lipid metabolism, functioning as a fuel gauge sensor. ACC and HMG-CoA reductase are well known to be substrates of AMPK; however, downstream from AMPK, their roles in glucose uptake and glycogen metabolism remain unclear. In this study, we identified GDE as an AMPK-binding protein by using a GST-AMPK pull-down assay. Coimmunoprecipitation of AMPK with GDE was observed not only in overexpression experiments but also endogenously (Fig. 1*B*). In addition, the β-subunit was demonstrated to be responsible for the association with GDE. Interestingly, the portion of the β-subunit that binds with GDE (amino acids 68–123 of AMPKβ1) is included in the sequence that reportedly associates with glycogen (amino acids 68–163 of AMPKβ1). Thus we suspected that the association between the β-subunit and GDE occurs via the binding of glycogen to both the β-subunit and GDE. However, W100G and K128Q, glycogen nonbinding mutants of the β1-subunit, fully retained the ability to bind with GDE, suggesting that the association between the β-subunit and GDE does not involve glycogen binding. Furthermore, we found that adding glycogen to the buffer did not alter the in vitro association between the β-subunit and GDE (data not shown). Taking these two observations into consideration, it is reasonable to assume that the association of the β-subunit of AMPK with GDE is direct.

GDE, a 160-kDa monomeric protein, is widely distributed in bacteria, yeasts, plants, and animals. GDE contains two independent catalytic activities, transferase and glucosidase (22, 23), that are responsible for glycogen degradation. Although glycogen phosphorylase degrades glycogen from its nonreducing ends, leaving dextrin with shortened chains, GDE transfers maltosyl units from the shortened chain to another chain employing its transferase activity. GDE then removes the glycosyl stub using its glucosidase activity. Genetic deficiency

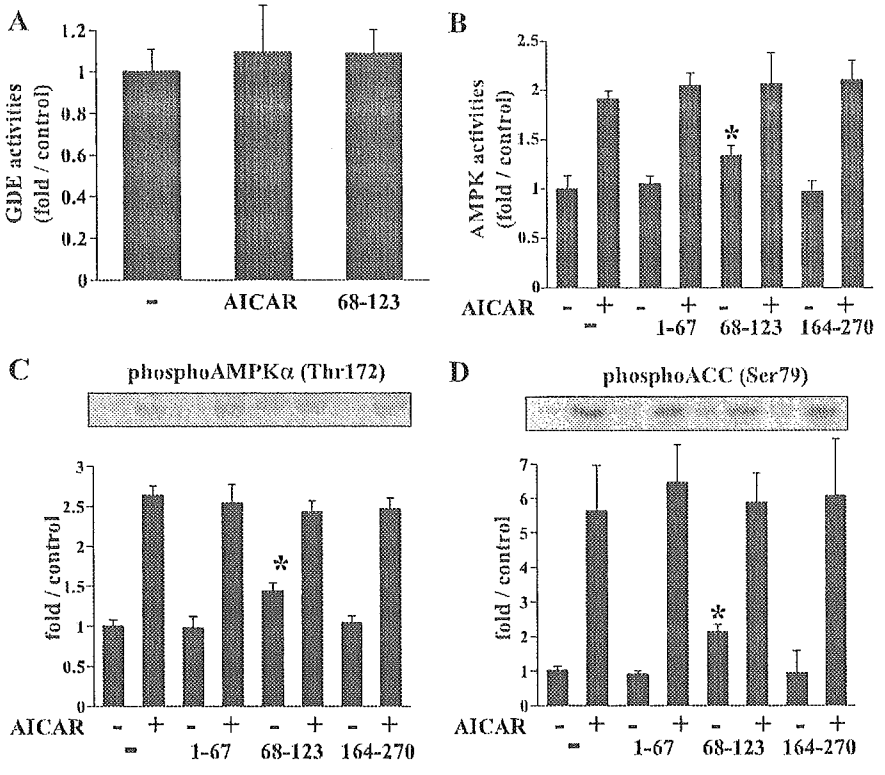

Fig. 4. Inhibition of association between AMPK and GDE increases basal phosphorylation of AMPKα and acetyl-CoA carboxylase (ACC) and also increases basal AMPK activity. *A*: after serum starvation, preincubation, and 5-aminoimidazole-4-carboxamide-1-β-d-ribofuranoside (AICAR) stimulation, as described in RESULTS, GDE-overexpressing COS-7 cells were collected with Tris buffer and then sonicated. Sonicated cells were centrifuged at 17,000 *g* for 20 min, and supernatants were immunoprecipitated with anti-Flag antibody. GDE activities in immunoprecipitants were assayed using glucosyl-β-cyclodextrin as substrate, as described in MATERIALS AND METHODS. Bars depict means ± SE of 3 independent experiments. *B*: COS-7 cells overexpressing amino acids 1–67, 68–123, or 164–270 of the β1-subunit were treated with or without 2 mmol/l AICAR for 30 min. Cells were then lysed and immunoprecipitated with anti-AMPKα antibody. AMPK activities in immunoprecipitants were assayed using SAMS peptide. Bars depict means ± SE of 3 independent experiments. *C* and *D*: COS-7 cells overexpressing amino acids 1–67, 68–123, or 164–270 of the β1-subunit were incubated with or without 2 mmol/l AICAR for 30 min. Cells were then lysed followed by SDS-PAGE and Western blotting using anti-phospho-AMPKα-Thr^{172} (*C*), and anti-phospho-ACC-Ser^{79} (*D*). *$P < 0.05$ vs. control cells (basal).

of GDE in humans is known to cause a type III glycogen storage disorder called Cori's disease (24), which is characterized by hepatomegaly, hypoglycemia, short stature, and muscle weakness (25–27).

A considerable portion of AMPK reportedly colocalizes with glycogen particles, although the physiological significance of this subcellular localization remains unclear. Our results suggest that this subcellular localization of AMPK may be due to binding to GDE but not glycogen or to binding both GDE and glycogen. In addition, we demonstrated herein that amino acids 68–123 of the β1-subunit contain the GDE binding domain. We also showed that overexpression of amino acids 68–123 of the β1-subunit effectively interrupts the binding of endogenous AMPK with GDE and significantly enhances AMPK activity. Thus it is very likely that the association with GDE suppresses the basal kinase activity of AMPK, although how release of the β-subunit from GDE affects the kinase activity of the α-subunit of AMPK remains unknown. We speculate that a decrease in glycogen content may induce dissociation of AMPK from GDE, thereby increasing AMPK activity, which leads to various metabolic actions, including increased glucose uptake and fatty acid oxidation. However, we did not examine the relationship between cellular glycogen contents and the association between AMPK and GDE herein. It is reasonable that upregulating AMPK activity would increase glucose uptake and fatty acid oxidation when cellular glycogen is in short supply. This hypothesis appears to be supported by a previous study showing AMPK activity to be higher in skeletal muscle containing less glycogen (12).

We also speculate that the localization of AMPK is important for its regulation of kinase activity. Many proteins, including protein phosphatase, bind to glycogen, and this binding determines their cellular localizations (8, 9). Furthermore, dissociation from glycogen may change certain protein interactions. AMPK is reportedly activated via phosphorylation of its α-subunit in response to ATP depletion, which is caused by muscle contraction, metabolic poisoning, oxidatative stress, hypoxia, and nutrient deprivation. Increased cellular AMP changes the conformation of the AMPKαβγ complex, revealing the Thr^{172} of the α-subunit to be phosphorylated by LKB-1 (28–30). Thus it is reasonable to speculate that the conformational change in AMPK induced by GDE binding affects the association of AMPK with LKB-1 or some other phosphatase(s). Unfortunately, however, we detected no significant change in the association between AMPK and GDE in response to either fasting or feeding of the mice or with serum starvation of COS-7 cells. Thus although this is the first study to demonstrate a direct association between AMPK and GDE, further studies are needed to clarify how this association is regulated. In addition, it is also necessary to elucidate the resultant physiological significance of this association, which may occur via the regulation of AMPK activity or subcellular localization.

GRANTS

This work was supported by a Grant-in-Aid for Suzuken Memorial foundation (04-042).

REFERENCES

1. **Hardie DG.** Minireview. The AMP-activated protein kinase cascade: the key sensor of cellular energy status. *Endocrinology* 144: 5179–5183, 2003.
2. **Carling D.** The AMP-activated protein kinase cascade–a unifying system for energy control. *Trends Biochem Sci* 29: 18–24, 2004.
3. **Rutter GA, Da Silva Xavier G, and Leclerc I.** Roles of 5'-AMP-activated protein kinase (AMPK) in mammalian glucose homoeostasis. *Biochem J* 375: 1–16, 2003.
4. **Musi N and Goodyear LJ.** AMP-activated protein kinase and muscle glucose uptake. *Acta Physiol Scand* 178: 337–345, 2003.
5. **MacLean PS, Zheng D, Jones JP, Olson AL, and Dohm GL.** Exercise-induced transcription of the muscle glucose transporter (GLUT 4) gene. *Biochem Biophys Res Commun* 292: 409–414, 2002.
6. **Buhl ES, Jessen N, Pold R, Ledet T, Flyvbjerg A, Pedersen SB, Pedersen O, Schmitz O, and Lund S.** Long-term AICAR administration reduces metabolic disturbances and lowers blood pressure in rats displaying features of the insulin resistance syndrome. *Diabetes* 51: 2199–2206, 2002.
7. **Wiatrowski HA, Van Denderen BJ, Berkey CD, Kemp BE, Stapleton D, and Carlson M.** Mutations in the gal83 glycogen-binding domain activate the snf1/gal83 kinase pathway by a glycogen-independent mechanism. *Mol Cell Biol* 24: 352–361, 2004.
8. **Polekhina G, Gupta A, Michell BJ, van Denderen B, Murthy S, Feil SC, Jennings IG, Campbell DJ, Witters LA, Parker MW, Kemp BE, and Stapleton D.** AMPK beta subunit targets metabolic stress sensing to glycogen. *Curr Biol* 13: 867–871, 2003.
9. **Hudson ER, Pan DA, James J, Lucocq JM, Hawley SA, Green KA, Baba O, Terashima T, and Hardie DG.** A novel domain in AMP-activated protein kinase causes glycogen storage bodies similar to those seen in hereditary cardiac arrhythmias. *Curr Biol* 13: 861–866, 2003.
10. **Halse R, Fryer LG, McCormack JG, Carling D, and Yeaman SJ.** Regulation of glycogen synthase by glucose and glycogen: a possible role for AMP-activated protein kinase. *Diabetes* 52: 9–15, 2003.
11. **Wojtaszewski JF, Nielsen JN, Jorgensen SB, Frosig C, Birk JB, and Richter EA.** Transgenic models—a scientific tool to understand exercise-induced metabolism: the regulatory role of AMPK (5'-AMP-activated protein kinase) in glucose transport and glycogen synthase activity in skeletal muscle. *Biochem Soc Trans* 31: 1290–1294, 2003.
12. **Wojtaszewski JF, Jorgensen SB, Hellsten Y, Hardie DG, and Richter EA.** Glycogen-dependent effects of 5-aminoimidazole-4-carboxamide (AICA)-riboside on AMP-activated protein kinase and glycogen synthase activities in rat skeletal muscle. *Diabetes* 51: 284–292, 2002.
13. **Milan D, Jeon JT, Looft C, Amarger V, Robic A, Thelander M, Rogel-Gaillard C, Paul S, Iannuccelli N, Rask L, Ronne H, Lundstrom K, Reinsch N, Gellin J, Kalm E, Roy PL, Chardon P, and Andersson L.** A mutation in PRKAG3 associated with excess glycogen content in pig skeletal muscle. *Science* 288: 1248–1251, 2000.
14. **Gollob MH.** Glycogen storage disease as a unifying mechanism of disease in the PRKAG2 cardiac syndrome. *Biochem Soc Trans* 31: 228–231, 2003.
15. **Sakoda H, Ogihara T, Anai M, Fujishiro M, Ono H, Onishi Y, Katagiri H, Abe M, Fukushima Y, Shojima N, Inukai K, Kikuchi M, Oka Y, and Asano T.** Activation of AMPK is essential for AICAR-induced glucose uptake by skeletal muscle but not adipocytes. *Am J Physiol Endocrinol Metab* 282: E1239–E1244, 2002.
16. **Sakoda H, Gotoh Y, Katagiri H, Kurokawa M, Ono H, Onishi Y, Anai M, Ogihara T, Fujishiro M, Fukushima Y, Abe M, Shojima N, Kikuchi M, Oka Y, Hirai H, and Asano T.** Differing roles of Akt and serum- and glucocorticoid-regulated kinase in glucose metabolism, DNA synthesis, and oncogenic activity. *J Biol Chem* 278: 25802–25807, 2003.
17. **Ogihara T, Isobe T, Ichimura T, Taoka M, Funaki M, Sakoda H, Onishi Y, Inukai K, Anai M, Fukushima Y, Kikuchi M, Yazaki Y, Oka Y, and Asano T.** 14-3-3 Protein binds to insulin receptor substrate-1, one of the binding sites of which is in the phosphotyrosine binding domain. *J Biol Chem* 272: 25267–25274, 1997.
18. **Liu W, de Castro ML, Takrama J, Bilous PT, Vinayagamoorthy T, Madsen NB, and Bleackley RC.** Molecular cloning, sequencing, and analysis of the cDNA for rabbit muscle glycogen debranching enzyme. *Arch Biochem Biophys* 306: 232–239, 1993.
19. **Nakayama A, Yamamoto K, and Tabata S.** Identification *of* the catalytic residues of bifunctional glycogen debranching enzyme, *J Biol Chem* 276: 28824–28828, 2001.
20. **Yanase M, Takata H, Takaha T, Kuriki T, Smith SM, and Okada S.** Cyclization reaction catalyzed by glycogen debranching enzyme (EC 2.4.1.25/EC 3.2.1.33) and its potential for cycloamylose production. *Appl Environ Microbiol* 68: 4233–4239, 2002.

21. **Sakoda H, Ogihara T, Anai M, Funaki M, Inukai K, Katagiri H, Fukushima Y, Onishi Y, Ono H, Yazaki Y, Kikuchi M, Oka Y, and Asano T.** No correlation of plasma cell 1 overexpression with insulin resistance in diabetic rats and 3T3-L1 adipocytes. *Diabetes* 48: 1365–1371, 1999.
22. **Liu W, Madsen NB, Braun C, and Withers SG.** Reassessment of the catalytic mechanism of glycogen debranching enzyme. *Biochemistry* 30: 1419–1424, 1991.
23. **Yang BZ, Ding JH, Enghild JJ, Bao Y, and Chen YT.** Molecular cloning and nucleotide sequence of cDNA encoding human muscle glycogen debranching enzyme. *J Biol Chem* 267: 9294–9299, 1992.
24. **Shen J, Bao Y, Liu HM, Lee P, Leonard JV, and Chen YT.** Mutations in exon 3 of the glycogen debranching enzyme gene are associated with glycogen storage disease type III that is differentially expressed in liver and muscle. *J Clin Invest* 98: 352–357, 1996.
25. **Chen YT, Bali D, and Sullivan J.** Prenatal diagnosis in glycogen storage diseases. *Prenat Diagn* 22: 357–359, 2002.
26. **Shen JJ and Chen YT.** Molecular characterization of glycogen storage disease type III. *Curr Mol Med* 2: 167–175, 2002.
27. **Wolfsdorf JI, Holm IA, and Weinstein DA.** Glycogen storage diseases. Phenotypic, genetic, and biochemical characteristics, and therapy. *Endocrinol Metab Clin North Am* 28: 801–823, 1999.
28. **Woods A, Johnstone SR, Dickerson K, Leiper FC, Fryer LG, Neumann D, Schlattner U, Wallimann T, Carlson M, and Carling D.** LKB1 is the upstream kinase in the AMP-activated protein kinase cascade. *Curr Biol* 13: 2004–2008, 2003.
29. **Hawley SA, Boudeau J, Reid JL, Mustard KJ, Udd L, Makela TP, Alessi DR, and Hardie DG.**Complexes between the LKB1 tumor suppressor, STRAD alpha/beta and MO25 alpha/beta are upstream kinases in the AMP-activated protein kinase cascade. *J Biol* 2, 28: 2003.
30. **Shaw RJ, Kosmatka M, Bardeesy N, Hurley RL, Witters LA, DePinho RA, and Cantley LC.** The tumor suppressor LKB1 kinase directly activates AMP-activated kinase and regulates apoptosis in response to energy stress. *Proc Natl Acad Sci USA* 101: 3329–3335, 2004.

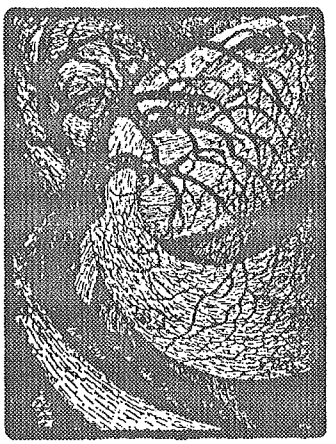

Adenosine Monophosphate-Activated Protein Kinase Suppresses Vascular Smooth Muscle Cell Proliferation Through the Inhibition of Cell Cycle Progression

Motoyuki Igata,* Hiroyuki Motoshima,* Kaku Tsuruzoe, Kanou Kojima, Takeshi Matsumura, Tatsuya Kondo, Tetsuya Taguchi, Kazuhiko Nakamaru, Miyuki Yano, Daisuke Kukidome, Kazuya Matsumoto, Tetsushi Toyonaga, Tomoichiro Asano, Takeshi Nishikawa, Eiichi Araki

Abstract—Vascular smooth muscle cell (VSMC) proliferation is a critical event in the development and progression of vascular diseases, including atherosclerosis. We investigated whether the activation of adenosine monophosphate-activated protein kinase (AMPK) could suppress VSMC proliferation and inhibit cell cycle progression. Treatment of human aortic smooth muscle cells (HASMCs) or isolated rabbit aortas with the AMPK activator 5-Aminoimidazole-4-carboxamide ribonucleoside (AICAR) induced phosphorylation of AMPK and acetyl Co-A carboxylase. AICAR significantly inhibited HASMC proliferation induced by both platelet-derived growth factor-BB (PDGF-BB) and fetal calf serum (FCS). Treatment with AICAR inhibited the phosphorylation of retinoblastoma gene product (Rb) induced by PDGF-BB or FCS, and increased the expression of cyclin-dependent kinase inhibitor $p21^{CIP}$ but not that of $p27^{KIP}$. Pharmacological inhibition of AMPK or overexpression of dominant negative-AMPK inhibited both the suppressive effect of AICAR on cell proliferation and the phosphorylation of Rb, suggesting that the effect of AICAR is mediated through the activation of AMPK. Cell cycle analysis in HASMCs showed that AICAR significantly increased cell population in G0/G1-phase and reduced that in S- and G2/M-phase, suggesting AICAR induced cell cycle arrest. AICAR increased both p53 protein and Ser-15 phosphorylated p53 in HASMCs, which were blocked by inhibition of AMPK. In isolated rabbit aortas, AICAR also increased Ser-15 phosphorylation and protein expression of p53 and inhibited Rb phosphorylation induced by FCS. These data suggest for the first time that AMPK suppresses VSMC proliferation via cell cycle regulation by p53 upregulation. Therefore, AMPK activation in VSMCs may be a therapoietic target for the prevention of vascular diseases. (*Circ Res.* 2005;97:837-844.)

Key Words: AMP-activated protein kinase ■ cell cycle arrest ■ p53 ■ p21 ■ AICAR

Vascular smooth muscle cell (VSMC) proliferation is one of the critical events in the development and progression of various vascular diseases, including atherosclerosis and restenosis after coronary intervention.[1] Mammalian cell proliferation is governed by the cell cycle.[2] Cell cycle progression is a tightly controlled event regulated positively by cyclin-dependent kinases (CDKs) and their cyclin-regulatory subunits,[3] and negatively by CDK inhibitors (CDKIs) and tumor suppressor genes.[4] Mitogenic factors bind to their receptors and initiate a series of events resulting in the activation of CDKs, which in turn regulates cell cycle progression and mitosis.[5]

The cell cycle entry of VSMCs is stimulated by a variety of growth factors produced from inflammatory cells, platelets, and the vascular cells where vascular injury occurs.[1] Although these growth factors, including platelet-derived growth factor (PDGF), basic fibroblast growth factor, insulin-like growth factor, and angiotensin II (Ang II), use distinct signaling pathways to promote DNA synthesis in VSMC, these signaling pathways must converge on common regulators of the cell cycle such as CDKs and CDKIs.[6] The final common pathway leading to G0/G1/S transition is the CDKs-induced hyperphosphorylation of the retinoblastoma gene product (Rb),[7] which functions as a molecular switch dedicating the cell to DNA replication. Hyperphosphorylation of Rb results in the release of the transcription factor E2F, which induces the expression of genes required for the progression through the S, G2, and M phases.[8] CDKIs such as $p21^{CIP}$ negatively regulate cell cycle progression by inhibiting cyclin/CDKs activity and phosphorylation of Rb, resulting in G1 arrest.[9] Progression of the cell cycle is therefore regulated by the balance between the levels and activities of cyclin-

Original received May 31, 2005; resubmission received August 9, 2005; revised resubmission received August 31, 2005; accepted August 31, 2005.

From the Department of Metabolic Medicine (M.I., H.M., K.T., K.K., T.M., T.K., T. Taguchi, K.N., M.Y., D.K., K.M., T. Toyonaga, T.N., E.A.), Faculty of Medical and Pharmaceutical Sciences, Kumamoto University, Kumamoto, and the Department of Physiological Chemistry and Metabolism (T.A.), Graduate School of Medicine, University of Tokyo, Japan.

*Both authors contributed equally to this work.

Correspondence to Hiroyuki Motoshima, Department of Metabolic Medicine, Faculty of Medical and Pharmaceutical Sciences, Kumamoto University, 1-1-1 Honjo, Kumamoto 860-8554, Japan. E-mail hmoto@gpo.kumamoto-u.ac.jp

Circulation Research is available at http://circres.ahajournals.org DOI: 10.1161/01.RES.0000185823.73556.06

CDK complexes, CDKIs, and other growth suppressor proteins such as p53.

Tumor suppressor p53 is tightly regulated by its phosphorylation state. Cellular stresses such as γ-irradiation induce Ser-15 phosphorylation of p53.[10,11] The phosphorylated p53 induces cell cycle arrest and/or apoptosis through the transcriptional regulation of p53 response genes such as $p21^{CIP}$.

Adenosine monophosphate-activated protein kinase (AMPK) plays a key role in the regulation of energy homeostasis and monitors cellular energy charge, acting as a "metabolic master switch" to regulate adenosine triphosphate concentrations in the face of stresses that reduce cellular energy levels.[12–14] AICAR (5-Aminoimidazole-4-carboxamide ribonucleoside) is a well-known activator of AMPK. AICAR is transported inside the cells through the adenosine transporter and phosphorylated by adenosine kinase[15] to form zeatin riboside-5-monophosphate (ZMP), which mimics the stimulatory action of AMP on AMPK.[16] Previous studies reported that AICAR could inhibit apoptosis in primary astrocytes[17] and endothelial cells.[18] On the other hand, AICAR has been reported to cause apoptosis in neuroblastoma cell lines[19] and B-cell chronic lymphocytic leukemia cells.[20]

Thus far, only 2 studies have reported the role of AMPK activation in VSMCs.[21,22] Whereas Rubin et al[21] reported the activation of AMPK with 2-deoxyglucose plus N_2, but not with AICAR, in rat carotid artery smooth muscle, Nagata et al[22] reported that AICAR activated AMPK in rat aortic SMCs and further inhibited Ang II-induced SMC proliferation. No information is available, however, on the effect of AICAR in human aortic SMCs (HASMCs). Therefore, in the present work, we determined whether AMPK activation by AICAR could suppress proliferation or induce apoptosis in HASMCs, and further investigated the mechanisms of AICAR-induced suppression of VSMC proliferation. We have found that AICAR exerts an antiproliferative effect through the activation of AMPK in HASMCs, and that the mechanism seems to involve cell cycle arrest through the upregulation of p53 and $p21^{CIP}$.

Materials and Methods

Cell Culture and Reagents

HASMCs were purchased from Clonetics (Walkersville, Md). For all experiments, early passaged (passages 4 to 7) SMCs were used. AICAR was obtained from Toronto Research Chemicals. We purchased 5′-amino-5′-deoxyadenosine (AMDA), dipyridamole, diethylmaleate (DEM), and PDGF-BB from Sigma.

Cell Proliferation Assay

We used 2 different methods, cell counting assay[23] and Alamar Blue assay[24] as described previously (see also expanded Materials and Methods available online at http://circres.ahajournals.org).

Determination of DNA Content Using Hoechst 33258 Dye

DNA content in SMCs was determined as an index for cell proliferation or for cytotoxity according to the instruction supplied by Thermo Labsystems (see also expanded Materials and Methods).

Experiments Using Adenoviral Vectors

An adenoviral vector expressing dominant negative (DN)-AMPK (Ad-DN-AMPK), which serves as a nonphosphorylatable T172A mutant of AMPK α-subunit[25] and contains a c-*myc* tag at the NH_2 terminus, was used to inhibit AMPK activity as described previously.[26] SMCs were infected with the indicated adenoviral vectors at 100 multiplicity of infection (100 MOI) for 2 hours. The medium was then changed to Dulbecco's modified eagle medium (DMEM) containing 0.2% fetal calf serum (FCS). After the incubation for 2 days, infected cells were stimulated with 10 ng/mL PDGF-BB or 15% FCS in the presence or absence of AICAR. In some experiments, cells were pretreated with AICAR for 4 hours. In experiments using inhibitors, inhibitors were added 30 minutes before AICAR treatment.

Cell Cycle Analysis

The fraction of cells present in each cell cycle phase (G0/G1, S, and G2/M) was determined by flow cytometry using a BD FACStar flow cytometer and ModiFit software from Verity House.

Detection of Apoptosis

A sandwich ELISA method was used to assess apoptosis using the Cell Death ELISA plus kit (Roche) as described previously.[27]

Western Blots

Western blotting was performed essentially as previously reported.[28]

Ex Vivo Experiments

Male Japanese white rabbits (Kyudo Co Ltd, Saga, Japan) were euthanized by overdose of Inactin. The descending thoracic aorta was rapidly excised and cleaned of connective tissues. The endothelium was removed by gently rubbing the vessel with wet cotton swab. The aorta was cut into 5-mm rings and the rings were cut open into strips. The aortic strips were stimulated without or with 15% FCS in the presence or absence of AICAR. After the stimulation, strips were homogenized in the lysis buffer. Western Blot analyses were performed as described above.

Experimental procedures for a real-time reverse transcription polymerase chain reaction (RT-PCR) analysis, a dual-luciferase assay for p53-dependent transcription, trypan blue exclusion assay, and detailed information for procedures described above are available in an expanded Materials and Methods section at http://circres.ahajournals.org.

Results

AICAR Suppresses Proliferation and DNA Synthesis of HASMCs Stimulated by PDGF-BB or 15% FCS

To determine the roles of AMPK on SMC proliferation, we first investigated the effect of AICAR on proliferation by the cell count assay. Treatment of HASMCs with PDGF-BB (10 ng/mL) or 15% FCS increased cell proliferation by ≈2.6-fold and ≈3.6-fold, respectively, compared with control cells incubated with 0.2% FCS. AICAR decreased the number of cells induced by PDGF-BB or 15% FCS in a dose-dependent manner (Figure 1A and 1B). Similar results were obtained in primary rabbit aortic SMCs (RASMCs) (supplemental Figure S1A and S1B).

We further investigated the inhibitory effect of AICAR on proliferation using Alamar Blue assay. Treatment with AICAR significantly reduced Alamar Blue fluorescence intensity in HASMCs stimulated with PDGF-BB or 15% FCS (Figure 1C). Microscopic observation after Alamar Blue assay confirmed that the decreased fluorescence intensity in AICAR-treated cells was due to the reduced cell number